Engineered cathode buffer layers for highly efficient organic solar cells: A Review

Swati Bishnoi[1,†], Ram Datt[2, †], Sandeep Arya[3], Sonal Gupta[4], Ramashanker Gupta[1,6], Wing Chung Tsoi[2], Shailesh N. Sharma [1], Shashikant P. Patole[5], Vinay Gupta[5,*]

[1]Advanced Materials and Devices Metrology Division, CSIR-National Physical Laboratory, Dr. K. S. Krishnan Marg, New Delhi, 110012, India

[2]SPECIFIC, Faculty of Science and Engineering, Swansea University, Bay Campus, Fabian Way, Swansea- SA1 8EN, United Kingdom

[3]Department of Physics, University of Jammu, Jammu, Jammu and Kashmir 180006, India

[4]Institute of Macromolecular Chemistry, Czech Academy of Sciences, 162 06 Prague 6, Czech Republic

[5]Department of Physics, Khalifa University of Science and Technology, P. O. Box 127788, Abu Dhabi, United Arab Emirates, Corresponding Author

[6]Academy of Scientific and Innovative Research (AcSIR), 201002 Ghaziabad, India

[†] S.B. and R.D. are co-first authors with equal contribution to this work.

drvinaygupta@netscape.net

Abstract:

This article presents an in-depth insight into the most efficient cathode buffer layers (CBLs) in conventional and inverted organic solar cells (OSCs). The CBL can play a critical role in improving the short circuit current density (J_{sc}) and fill factor (FF) of the devices by

minimizing the contact resistance and reducing charge recombination at electrode/photoactive layer interface, resulting in the efficient extraction of charge carriers and therefore improving the power conversion efficiency (PCE). This review explores CBL with respect to its effect on the physics of a device and electronic processes at the interface of CBL/photoactive layer and its impact on the overall performance of solar cells. Besides this, we have discussed in detail the role of CBL, its chemical composition, morphology, thickness, dopants, deposition conditions, etc. and their corresponding effects on the device performance in both conventional and inverted OSCs. Finally, we have summarized a few CBLs that provided the best performance and discussed their chemical structures. This article will benefit the researchers working in the domain of solar cells by providing an understanding of the CBL layers, along with their interfacial working mechanism.

Keywords: Cathode buffer layer, organic solar cell, power conversion efficiency, interfacial layer, electron transport layer.

1. Introduction:

Energy is the driving force behind all the facilities available for human activities to make life comfortable on the Earth, and its demand is increasing equivalently with the upturn in the standard of human living. Traditionally, fossil fuels such as coal and natural oil have maximally impacted the power generation throughout the globe. Unfortunately, fossil fuels are also the primary sources of greenhouse gases and are increasing as a result of human activities that have necessitated enhanced power generation.[1] The Inter-governmental Panel on Climate Change (IPCC) has warned about the global temperature that will rise by 4°C to 5.8°C by the end of the century; carbon dioxide (CO_2) too will increase up to 1099 ppm by 2100s. [2] All this will

2

severely impact the environment in terms of melting glaciers, rising sea levels, and global warming, etc. This has led the research focus on renewable energy alternative sources such as solar energy, wind energy, and geothermal, etc., in which solar energy is an abundant and attractive for photovoltaic (PV) application. In photovoltaic, silicon (polycrystalline, monocrystalline, and amorphous), copper indium gallium (di) selenide (CIGS), gallium arsenide (GaAs), and cadmium telluride (CdTe), heterojunction with intrinsic thin-layer (HIT) based PV technologies are being used worldwide in which silicon- wafer-based solar cells account for about 94 % of the total production. [3–7] However, the high cost of inorganic photovoltaic has prevented these technologies from having a significant impact on global energy production. The main disadvantage of these solar cell technologies is the high purity environment needed for device handling and processing. [8,9] The energy and cost required for the material processing and device fabrication are comparatively high, which limits its effectiveness as an alternate energy source. The perovskite solar cells (PSCs) and dye-sensitized solar cells (DSSCs) are also being studied as potential alternatives. [10,11] DSSCs could be considered as an option for future solar cell technology, nonetheless it suffers from several drawbacks like low PCE as well as it includes the use of liquid electrolytes and that are difficult to control at high temperature. [12,13] Recently, PSCs have shown remarkable potential in terms of efficiency and it can be used as a future technology for harvesting the solar light with their comparable PCE to silicon solar technology within a short span.[14] However, currently, PSCs possess some critical problems, like; short lifetime, environmental sensitivity, and toxicity, which are the major hindrances in their commercialization. [15,16] The OSCs are continuously attaining remarkable attention in the area of photovoltaics owing to their ease of fabrication with substrate flexibility, and low cost large- scale production. [17–23] Moreover, the chemical flexibility for modifications in organic

semiconductors via chemical synthesis drives the research interest in both academia and industry fields. [24,25] Besides this, OSCs are lightweight, flexible, disposable, green, and can be customized on the molecular level to tune the band energy. According to the first report on OSCs in 1976s by Merritt et al. [26], the film (100- 1000 Å) of organic dye (hydroxy squarylium) was used to prepared the active layer. It resulted in PCE of 0.1 % at 0.14mW/cm^2 (AM0) input intensity and decreased to 0.02 % at 135mW/cm^2. The PCE was very low due to the high binding energy of the generated excitons (bound electron hole pair), and the separation of charge carriers was also inefficient. This drawback was overcame in 1986 when Tang introduced the concept of layer by layer coating of donor and acceptor together in a single cell, and it resulted in enhancement of PCE up to 1 %. [27] Figure 1 (a-c) shows the OSCs donor-acceptor molecules layer structure evolution. The concept of individual donor and acceptor layers (also known as bilayer structure) has been widely used in many photovoltaic cells, including dye/dye, polymer/polymer, and polymer/dye, etc. [28] The bilayer structure of OSCs exhibited certain limitations, such as short lifetime and short diffusion length of charge carriers. The next breakthrough came in 1995 when the concept of bulk-hetrojunction (BHJ) in OSCs was introduced by Heeger and Wudl [29] in which two organic semiconductors; an electron-donating and strong light-absorbing conjugated polymer (MEH-PVV) and a fullerene derivative PCBM as an acceptor material were used in a single blend (solution) to form a randomly mixed network with numerous interfaces (heterojunction) while coating it as layer. It was the first approach to overcome the milestone of 1 % PCE in organic photovoltaic. Furthermore, the last two decades were the golden period of OSCs, and recently the PCE crossed the barrier of 18 %. [30] This period witnessed the evolution of device structures, active layer stacking technique, development of buffer layers, donor and acceptor materials, and encapsulation methods, etc. There are

primarily two types of device geometries, called as conventional (Figure 1e) and the inverted (Figure 1f). The buffer layers used in OSCs are well known as a cathode buffer layer (CBL) or electron transport layer (ETL) or electron selective layer (ESL), or electron collection layer (ECL) and anode buffer layer (ABL) or hole transport layer (HTL) or hole selective layer (HSL), or hole collection layer (HCL). These have played an important role in PCE enhancement by increasing the charge carrier transport property, reduced recombination losses at active layer and electrode interface, and modified an electrode work function, etc. [30–32]. There are a few review articles available on organic solar cells that cover the development of interfacial layers, active layer materials, and development of the OSCs device structures, along with their effect on device performance [33–44]. However, the role of buffer layers, and their impact on the OSCs performance have not been well studied and summarized systematically. In particular, we have focused on cathode buffer layer materials, which have made substantial progress for enhancing the performance in conventional as well as inverted device structure in the last two decades.. Therefore, the present article deals with the development of different categories of CBL materials and their corresponding effects on device performance in both conventional and inverted type OSCs devices. The review covers an overview of the thermally evaporated as well as solution processable CBL materials reported so far.

Organic solar cells working mechanism

An organic or plastic solar cell is a special class of PV cells that relies on semiconductive organic molecules (polymer/small molecules) as light absorption and charge carrier generation, by the photovoltaic effect. [45] The small molecules/polymers have large conjugated systems of carbon atoms, covalently bonded with alternating single and double bonds. The P_z -orbital of the hydrocarbon's electrons delocalize and results in a delocalized bonding π orbital with a π^*

antibonding orbital. The highest occupied molecule orbital (HOMO) stands for the delocalized π orbital, and the π* orbitals form the low unoccupied molecular orbital (LUMO). The HOMO and LUMO separation is considered as the bandgap in the organic semiconductor materials. This bandgap is typically in a order of 1-3 eV. After a photon gets absorbed in the active layer, an electron is excited from HOMO to the LUMO, and leaves an empty electron spot in the HOMO. This spot is also known as a hole. The excited electrons and holes form a neutral state called an exciton. The exciton must be dissociated to free charge carriers and produce electricity. After dissociation, the electrons and holes move towards respective electrodes. Figure 2 and Figure 3 show the architecture and working mechanism of a typical organic bulk heterojunction solar cell, respectively. Scheme 1, 2 and 3 show the molecular structures of donor, acceptor, and organic CBL layer molecules presented in this review.
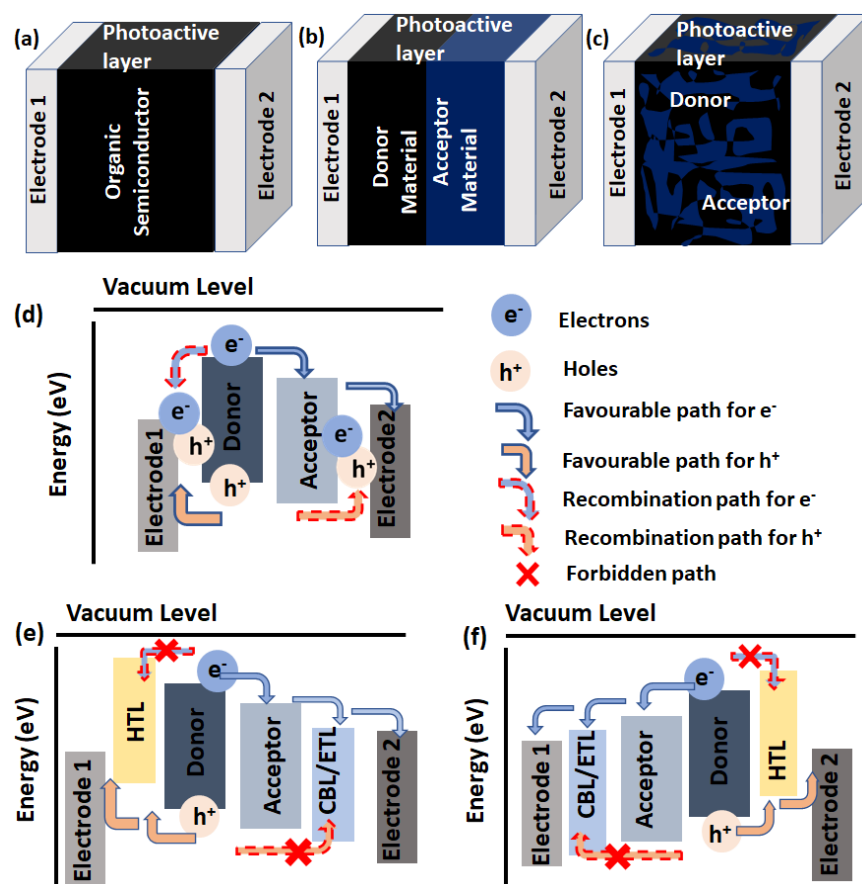
Figure (1): Schematic device structure of (a) single layer homojunction (b) bilayer heterojunction and (c) bulk heterojunction, based OSCs. The demonstraton of (d) recombination without buffer layer at electrode-active layer interface. The reduction of recombination at electrode-active layer interface by introducing buffer layers in (e) conventional, and (f) inverted device geometry.
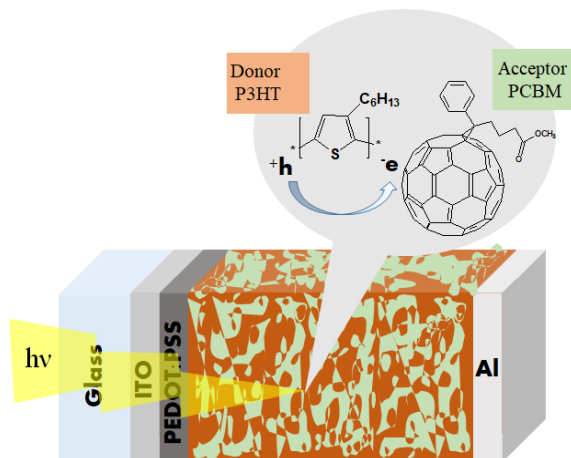

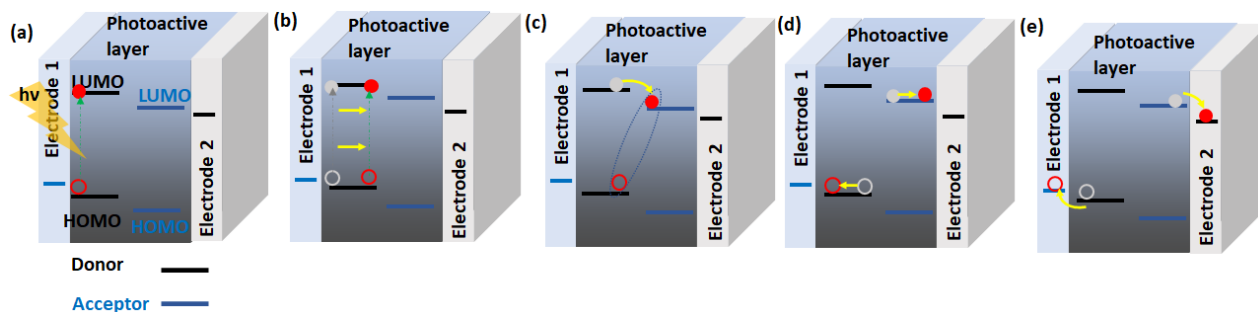Figure (2): Architecture of a conventional organic solar cell device.

Figure (3): Illustration of the major steps of the working mechanism in organic solar cell, which are as follows: (a) light absorption and exciton generation, (b) exciton diffusion, (c) exciton dissociation, (d) charge transport, and (e) the charge extraction to the electrodes.

Apart from donor/acceptor interface, the properties of organic/metal interface also plays an important role in determining the device performance. Without any surface modification, a contact between organic molecule and metallic electrodes is generally non-ohmic and that leads

to charge carriers accumulation and recombination at active layer/electrode interface. [46,47] Moreover, the unfavourable energy level of photoactive layer and electrode leads to a loss in the collection of charge carriers at electrodes. [48,49] Figure 1 (d-f) shows the charge carrier recombination at active layer-electrode interface and the way to reduce it by using buffer layers (charge carrier transport layers). Substantial efforts have been made to modify the organic/electrode interface for efficient charge extraction. This is often done by inserting the buffer layers , at anode and cathode side. The buffer layers can strongly affect the properties of the active layer/electrode interface by inducing interfacial charge redistributions and geometry modifications. In other words, buffer materials can be used to modified the active layer/electrode interfaces. In this article, the CBL and ABL terms are used for the sake of clarity for electron and hole transport layer, respectively and the CBL materials are discussed in details.

Anode Buffer Layer (ABL)

The primary task of the anode is the extraction of photogenerated holes from the active layer. In general, a transparent conductive oxide (TCO) substrates such as indium tin oxide (ITO), fluorine-doped tin oxide (FTO), and aluminum-doped zinc oxide (AZO), etc. coated glasses are used as anode (in conventional). An ITO has a favorable work function (~4.7 eV) with respect to the typical energy levels of the active layer materials; hence it can collect both positive and negative carriers. Therefore, ITO cannot provide the required selectivity. In addition, for polycrystalline ITO thin films, it induces a significant surface roughness at the nanometer scale. [50,51] This surface roughness is regarded as a major cause of leakage current in the resultant devices. [52] Also, ITO electrodes were reported to interact chemically with the organic material, and that contributes towards the degradation of OSCs device performances. [51,53,54] By taking all these factors into consideration, an anode buffer layer coating is needed, and it should fulfill the

8

following requirements: (1) establish ohmic contact with the donor material; (2) transport positive charge carriers efficiently (hole transporting); (3) block negative carriers (electron blocking); (4) smoothen the ITO surface to reduce surface recombination; (5) should be stable and transparent. [21,55] The PEDOT: PSS is the most commonly used anode layer, and is a *p*-type semiconductor with work function of 5.2 eV. It allows a favorable band alignment with the HOMO level of the donor molecules. Furthermore, it also forms a smooth film and improves the contact between the polymer and the ITO, thereby preventing any short-circuit probability due to ITO surface roughness. Unfortunately, the acidic nature of PEDOT:PSS and its UV prone degradation have restricted its further use. [54–56] Moreover, the processing method of PEDOT: PSS leads to water insertion in the active layer, as it is coated from a water based solution. [57,58] Even after baking, water traces persist on the surface owing to its hygroscopic nature, hence it can be a potential threat for the device lifetime. This has led to the emergence of alternative anode buffer layers including small organic molecules, polymers, metals, and inorganic metal oxides [61, 62]. [59, 60]

Cathode Buffer Layer (CBL)

The primary role of a CBL is to facilitate the collection of electrons at electrode. For smooth device functioning, CBL also performs several other crucial tasks, such as; (1) forming an electron selective and transport interlayer, (2) forming an ohmic contact with the aceptor molecule; (3) transporting negative charge carriers efficiently (electron-transporting); (4) blocking the reverse charge carriers (5) protecting the active layer in conventional device structure from the hot metal atoms during thermal deposition of the cathode; For efficient OSCs, the selection of an appropriate CBL to optimize the electron collection and transport is highly important. An ideal CBL should be good at electron extraction and transport. It must have a

suitable energy level that facilitates electron transport, with high transparency, good compactness, and high stability. Several commonly used cathode buffer layers were first established for organic light-emitting diodes and then transferred to OSCs fabrication. In the past few years, several materials have been explored as CBL in conventional and inverted type OSCs and these are summarized in Figure (4). A brief detail of some most efficient used CBLs are given below in Table (1).

Table 1: Cathode buffer layers work function, optimized thickness, and their deposition process.

Cathode buffer layers	Work function (eV)	Optimized thickness (nm)	Deposition process	Implemented in conventional/inverted	Ref.
Barium (Ba)	2.7	20	Thermal evaporation	Conventional	[61]
Calcium (Ca)	2.9	20	Thermal evaporation	Both	[62]
Cesium carbonate (Cs_2CO_3)	1.9	1	Thermal evaporation	Both	[63]
Aluminium oxide (Al_2O_3)	3.89- 4.02	2	Thermal evaporation	Inverted	[64]
Zinc oxide (ZnO)	4.3-4.5	30-60	Spin coating	Both	[65]
Titanium dioxide (TiO_2)	4.5- 4.6	10-20 nm	Spin coating	Both	[66]

Carbonate | Metals | acetylacetonates | Alkali Metals | Oxides | Quantum dots | Organic molecules

Carbonate	Metals	acetylacetonates	Alkali Metals	Oxides	Quantum dots	Organic molecules
Cs_2CO_3	Ca	Zirconium	LiF	TiO_2	ZnS	BCP
	Ba	Hafnium	NaF	CaO	CdSe	CuPc
		Aluminium	CsF	ZrO	MoS_2	TIPD
			KF	ZnO	InP	DCDA
				SnO_2	QQDs	PFN
				Al_2O_3	$CuGaSe_2$	PTE
						PEIE
						PEI
						WPF-6-oxy-F

Cathode buffer layers used for following device structure
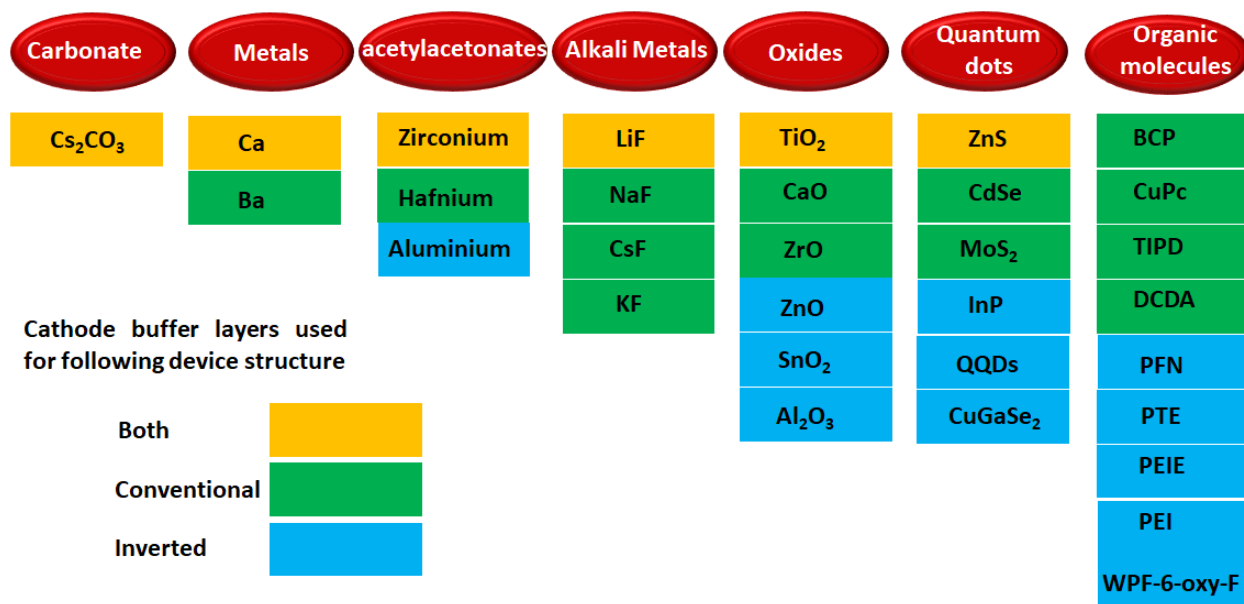
Both

Conventional

Inverted

Figure (4): Schematic diagram showing the commonly used CBL materials in conventional and inverted OSCs.

2. Materials for cathode buffer layer: conventional architecture

2.1 Oxides, acetylacetonate and carbonates as CBL

Oxides

Titanium oxide (TiO₂)

Over the past few years, many semiconducting metal oxides have been explored as CBL materials in the OSCs. TiO_2 is one of the commonly used oxide as CBL owing to its unique optical properties. [67] Peng et al. [68] proposed that the overall PCE of the OSCs device strongly depends on the TiO_2 film morphology. It was reported that TiO_2's well-defined and

homogeneous morphology was beneficial for charge separation and it helped in improving the device performance. Morphological characterization revealed that the TiO_2 film with homogenous morphology has better PCE of 3.56 % than non-homogenous film (PCE~ 1.90 %). It was also observed that the electron mobility in the TiO_2 film increases due to its crystallized nature after the heat treatment. [69] In 2006, a research group applied the solution-based titanium oxide (TiO_x) layer on top of the polymer: fullerene active layer. [70] By introducing TiO_x, the PCE of the resultant devices increases by approximately 50 % than the control device. The solution-processed TiO_x buffer layer serves as a multifunctional layer, such as an electron transport layer, an oxygen barrier, and an optical spacer. [71,72] Thus, it contributes to an efficiency improvement as well as enhances the stability of OSCs. For further improvement in the performance of TiO_2 based CBL, caesium (Cs) was doped in TiO_2. Park et al. [73] prepared the TiO_2: Cs by mixing cesium carbonate (Cs_2CO_3) solution into TiO_2 solution. The TiO_2: Cs shows stable nanostructure morphology. It resulted in the lowering work function of TiO_2, thus enabling efficient electron extraction. The conduction band (CB) of TiO_2 is 4.3 eV, slightly higher than aluminum (Al) electrode work function (4.2 eV), resulting in unfavorable electron extraction from the active layer to the electrode, and a S-shape in measured J–V characteristic was observed. On the other hand, CB level of the TiO_2: Cs layer (3.93 eV) is lower than Al work function and it facilitated the electron transport from the active layer to cathode. The devices (ITO/PEDOT: PSS/ P3HT: PCBM/CBL/Al) with TiO_2: Cs layer, has shown a considerable enhancement in the V_{oc} from 0.46 to 0.58 V, J_{sc} from 10.48 to 10.76 mA/cm^2, and FF from 0. 50 to 0.67. Thus, the PCE was achieved up to 4.2% for TiO_2: Cs layer, than 2.4 % for control device. Sun et al. [74], also reported the TiO_x interlayer with PCDTBT: $PC_{70}BM$ blend system, and the device delivered PCE upto 6.50%. Hadipour et al. [75] introduced a solution processable

TiO$_x$ layer, and it does not require any post-annealing. They demonstrated that the performance of the resultant device was comparable to a calcium (Ca) ETL based device, highlighting that the energy level positioning of TiO$_x$ as CBL is favorable for P3HT and PCDTBT donor molecules. It was concluded that the properties of the deposited TiO$_x$ remain unaltered, whether deposition was done in glove-box or in air. Thus, exploring their potentiality for roll-to-roll manufacturing.

Zinc oxide (ZnO)

Kyaw et al. [76] introduced the ZnO nanoparticles as CBL in the conventional device (Figure 5a), it acted as an optical spacer and enhanced the absorption within the active layer. The ZnO formed the favorable energy level (Figure 5b) for electron collection and transport them towards the electrode. The improvement has perceived in the J$_{sc}$ (13.4 to 15.5 mA/cm^2), V$_{oc}$ (0.795 to 0.799 V), and FF (0.56 to 0.72), which is related to the enhancement of charge collection and recombination reduction at electrodes, Figure 5c shows J-V characteristics of ZnO-based and control devices.
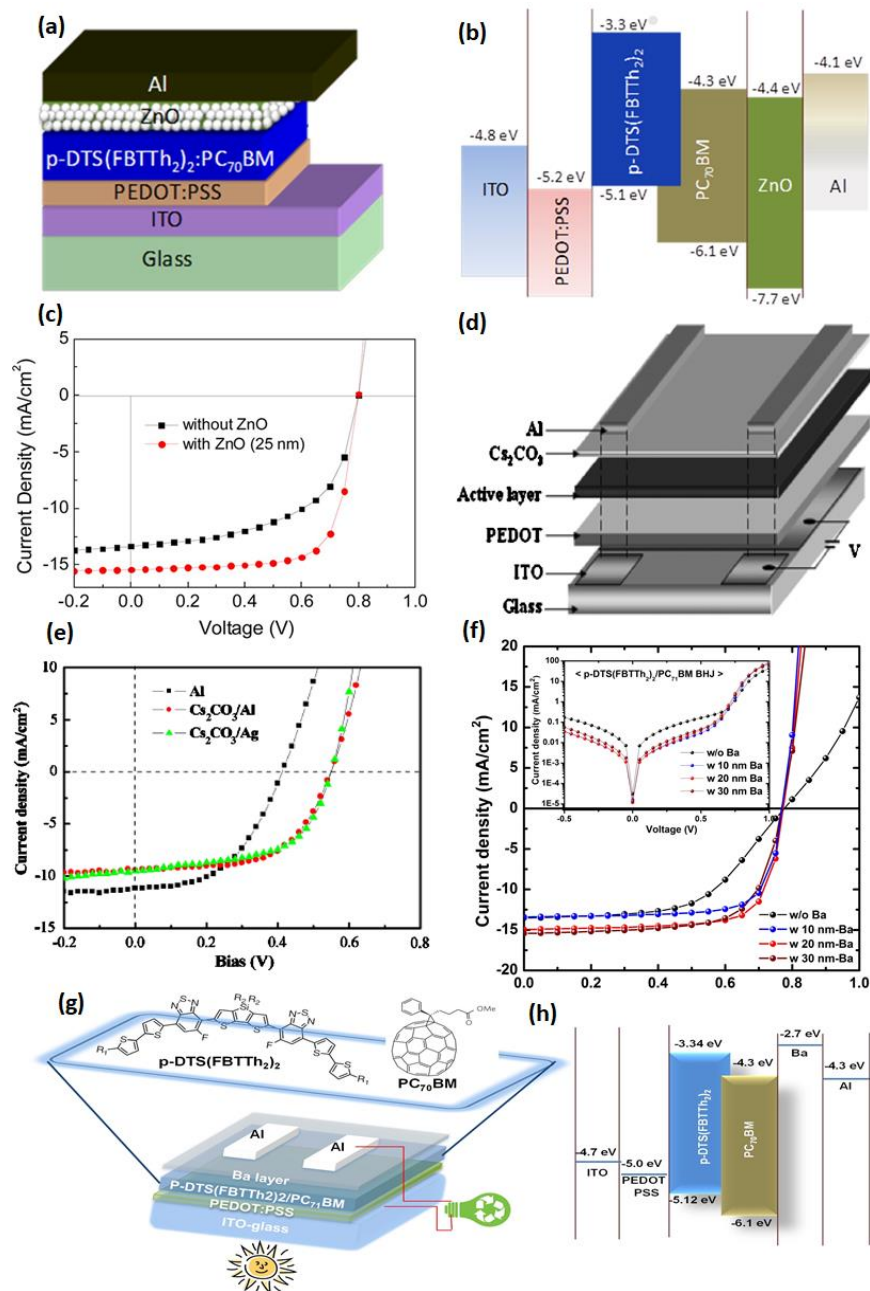
Figure (5): (a) Device structure of ZnO film as CBL and p-DTS(FBTTh$_2$)$_2$: PC$_{70}$BM as active layer, (b) Schematic illustration of the energy level diagram of components used in OSCs, showing ZnO film has favorable energy level for electron collection (c) J–V characteristics of with and without ZnO film at optimized active layer thichness of 100 nm. Reproduced with permission from ref. [76]. Copyright © 2006, American Chemical Society. (d) Cs$_2$CO$_3$ CBL

based OSCs schematic device structure, (e) J-V plot of the fabricated device (with and without Cs$_2$CO$_3$). Reproduced with permission from ref. [63], Copyright © 2008, AIP Publishing. p-DTS(FBTTh$_2$)$_2$: PC$_{71}$BM device (f) J-V characteristics (inset dark J-V characteristics), (g) device structure (h) Energy level diagram. Adapted from CC-BY open access publications (CC-BY license:3.0) ref. [61], Copyright © 2013, Gupta et al.

Zirconium Oxide (ZrO$_X$)

Chang et al. [77] studied the ZrO$_x$ based CBL and also reported CTAB (cetyltrimethylammonium bromide (CTAB) doped ZrO$_x$. The *n*-doped ZrO$_x$ CBL was easy to fabricate, and required no thermal annealing or any other post-treatment. Also, ZrO$_x$ shows good electrical conductivity, significant ambient stability, effective work function modulation of Ag electrode, relative weak thickness-dependent performance property, and compatible with a variety of active layer molecules. They studied the device performance with two different blend systems of PDPP-TBT: PC$_{71}$BM, and PTB7: PC$_{71}$BM. For PTB7: PC$_{71}$BM blend system, with undoped ZrO$_x$ layer, the PCE was 2.5% and was enhanced to 9.3 % for CTAB doped ZrO$_x$ CBL- based device. The CTAB-doped ZrO$_x$ layer has effectively reduced the cathode work function (WF) from 4.21 (ZrO$_x$/Ag) to 3.72 (CTAB-doped ZrO$_x$/Ag) eV. This reduction in cathode WF provides better energy level matching with an acceptor and benefitted the charge collection which results in an improvement in the J$_{sc}$, FF, as well as V$_{oc}$. The results are summarized in Table 2.

Table 2: A summary of calcium and zirconium oxide CBL based reported device parameters.

Device structure	Active layer	CBL	V$_{oc}$ (V)	J$_{sc}$ (mA/cm^2)	FF	PCE (%)	Ref
ITO/PEDOT:	P3HT: PC$_{60}$BM	-	0.56	9.55	0.49	2.65	[78]

PSS/Active layer/CBL/Al		Ca	0.60	9.95	0.62	3.75	
		a-ZrAcac	0.60	10.66	0.66	4.23	
	PBDTBDD: PC$_{60}$BM	-	0.78	12.10	0.60	5.72	
		Ca	0.86	12.06	0.70	7.34	
		a-ZrAcac	0.88	14.28	0.69	8.75	
	PBT1: PC$_{70}$BM	-	0.55	9.11	0.56	2.83	
		Ca	0.58	10.71	0.62	3.88	
		a-ZrAcac	0.60	10.73	0.62	4.01	
	P3HT: PC$_{70}$BM	-	0.70	9.50	0.58	3.92	
		Ca	0.86	11.44	0.64	6.34	
		a-ZrAcac	0.88	11.68	0.68	7.06	
	PBDTTT-C-T: PC$_{60}$BM	-	0.68	13.47	0.49	4.55	
		Ca	0.76	15.76	0.60	7.22	
		a-ZrAcac	0.79	15.95	0.60	7.55	
ITO/PEDOT: PSS/Active layer/ CBL/ Ag	PTB7: PC$_{71}$BM	ZrO$_x$	0.53	12.67	0.47	3.18	[77]
		-	0.24	3.21	0.15	0.12	
		CTAB-doped ZrO$_x$	0.73	16.87	0.73	9.30	
		CTAB	0.73	15.86	0.70	8.20	
ITO/CBL / Active layer/ MoO$_3$/Ag	C$_{60}$: CuPc	-	0.35	2.93	0.37	0.39	[79]
		Ca	0.39	2.99	0.54	0.64	

Calcium oxide (CaO)

Zhao et al. [80] explored the calcium oxide (CaO) as a CBL in P3HT: $PC_{61}BM$ active layer based OSCs. This group reported an enhancement in FF while introducing the CaO CBLs (1 nm thick) in the ITO/PEDOT: PSS/P3HT:PCBM/CBL/Al device structure. The control devices has V_{oc}, J_{sc}, and FF of 0.49 V, 8.35 mA/cm^2, and FF of 0.52, which contributed to generate the PCE up to 2.14 %. While after introducing the thin layer of CaO between active layer and Al an improved device performance parameters were obtained. The V_{oc}, J_{sc}, and FF were 0.57 V, 8.53 mA/cm^2, and 0.59, respectively, and the PCE was improved up to 2.98 %. An improvement in FF and V_{oc} showed that CaO CBL film reduced the leakage current.[81] Although the post annealing of P3HT: PCBM blend system has been reported an improvement in the device performance.[82] Unfortunately, in case of CaO CBL device, the post-anealing did not improve the device performance and the reason maybe the post-annealing destroyed the connection between Al and active layer by creating the discontinuity in the CaO film.

Zirconium and hafnium acetylacetonate

The zirconium and hafnium (IV) acetylacetonate as a solution processable CBL have been studied for conventional OSCs. Tan et al. [78] studied the solution-processed zirconium acetylacetonate (a-ZrAcac) as a CBL and it showed good compatibility with a variety of donor materials such as P3HT, PBT1, PBDTTT-C-T, and PBDTBDD with $PC_{60}BM$, and $PC_{70}BM$ acceptors. The PCE of OSCs for these donor materials were enormously enhanced after inserting a-ZrAcac as CBL than the control as well as Ca CBL based devices. It was also observed that the a-ZrAcac buffer layer helped in reducing the series resistance, and as a result enhanced the photogenerated current. Besides the device performance, an a-ZrAcac CBL has also improved the long term stability of non-encapsulated OSCs (P3HT: $PC_{60}BM$) under inert environment than Ca CBL based devices. Hancox et al. [83] proposed the a-ZrAcac for small molecule OSCs and it

can be processed in an air as well as in inert environment. The performance parameters of a-ZrAcac CBL based devices are summarized in Table 2. Yu et al. [84] introduced the hafnium(IV) acetylacetonate (Hf(acac)$_4$) with different donor-acceptor blend system. In PBDTBDD:PC$_{60}$BM and P3HT:PC$_{60}$BM blend system, the PCE have improved from 5.84 to 7.38 % and 2.94 to 4.02 %, respectively, by using ITO/PEDOT: PSS/Active layer/Hf(acac)$_4$/Al device structure. It was reported that Hf(acac)$_4$ low fermi level (-3.86 eV) lies near to acceptor (PC$_{60}$BM) LUMO energy (-3.90 eV), and it could be the reason to form energetically favorable electron extraction path from acceptor to electrode. Moreover, the Hf(acac)$_4$ has HOMO energy level (-6.64 eV) lower than PC$_{60}$BM (-5.90 eV), and it helps to block the holes extraction and efficiently works as CBL film.

Cesium carbonate (Cs$_2$CO$_3$)

The cesium carbonate (Cs$_2$CO$_3$) as an electron injection layer has been effectively studied for OLED application by the Canon group, and it is also expored for OSCs. Chen et al. [63] introduced the Cs$_2$CO$_3$ as a CBL in conventional device structure (Figure 5d). For the control device (Figure 5e), the V$_{oc}$, J$_{sc}$, and FF were 0.41 V, 11.2 mA/cm^2, 0.50, which resulted in the PCE of 2.3%. However, for Cs$_2$CO$_3$ device, the J$_{sc}$ was decreased slightly to 9.5 mA/cm^2, whereas the V$_{oc}$ and FF were enhanced to 0.56 V and 0.60, respectively. The insertion of CBL reduced the contact resistance between the electrodes and active layer, and as a result, device FF gets improved. The study suggested Cs$_2$CO$_3$ as a promising interlayer candidate for improving device performance. Huang et al. [85] comprehensively studied the origin of the low work function of nanostructured layers of Cs$_2$CO$_3$ film prepared by solution deposition and thermal evaporation. It is reported that the thermally evaporated Cs$_2$CO$_3$ decomposes into CsO$_2$ and cesium suboxides, and showed an intrinsically low work function. As a result, devices fabricated

using thermally evaporated Cs_2CO_3 are relatively insensitive to the choice of the cathode metal. However, devices prepared using solution-processed Cs_2CO_3 exhibit high efficiency with Al is used as the cathode metal. The result further confirms that Cs_2CO_3/Al can form a better ohmic contact with the organic layer, and thereby reduce the device series resistance.

2.2 Low work function metals as CBL

Calcium (Ca)

Calcium as an CBL has been explored in various conventional and inverted architecture based OSCs. The Ca has a work function of 2.9 eV, and it is favorable for forming ohmic contact between Ca and acceptor (PCBM) and rectifying contact with the donor (P3HT). As a result, Ca passes the electrons and blocks the holes towards the cathode. The researchers suggested the enhancement of device performance after inserting Ca as a CBL. Frisch et al. [86] reported the Ca as CBL in ITO/PEDOT: PSS/ P3HT: PFTBTT/CBL/Al device structure, and it shows highest PCE of 0.5 %, which was more than the control device (PCE~ 0.06%). Ju et al. [87] also introduced the Ca as CBL in the ITO/PEDOT: PSS/ PCDTBT: $PC_{71}BM$/CBL/Al device structure. The Ca interlayer based device delivered J_{sc}, V_{oc}, FF, and PCE of 10.93 mA/cm^2, 0.85 V, 0.46, and 4.31 %, respectively. In contrast, the devices without Ca interlayer exhibit low photovoltaic performance: V_{oc} = 0.80 V, J_{sc} = 10.29 mA/cm^2, FF = 0.40, and PCE = 3.37 %, apparently, the device performance is significantly improved by the Ca interlayer. Besides this, the Ca can induce a stronger dipole moment and band bending, and it can facilitate electron extraction and also help in hole blocking at cathode/polymer interface, leading to less non-geminate recombination. Gupta et al. [88] reported Ca as CBL in the ITO/PEDOT: PSS/ DTG

(FBT$_2$Th$_2$)$_2$: PC$_{71}$BM/CBL/Al device structure, and under optimized condition, PCE of 9.1 % was achieved in OSCs.

Barium (Ba)

Besides Ca, Ba as CBL was introduced in a small-molecule OSCs composed of p-DTS(FBTTh$_2$)$_2$)/ PC$_{71}$BM as an active layer. A FF of 0.75, which was one of the highest values reported for an OSCs, in the ITO/PEDOT: PSS/ DTS(FBTTh$_2$)$_2$): PC$_{71}$BM/Ba/Al device, and the PCE of 9.02 % achieved, which was of 46 % higher than control device [61]. Different thicknesses of Ba (10, 20, 30 nm) has been investigated, after inserting the Ba (10 nm), the device performance was improved considerably. For a similar thickness of Ca layer, the device exhibited J$_{sc}$ of 13.90 mA/cm^2, FF of 0.64, and a PCE of 7.01 %. An increase in the thickness of Ba cathode interlayer to 20 nm improved the PCE to 8.57 % with FF 0.74, whereas 20 nm Ca led to a PCE of 7.58 % with FF 0.67. The main changes were reported in FF after deposition of Ba that attributed to improved device performace by increasing the shunt resistance and reducing the series resistance. Figure 5 (f-h) shows the energy band diagram, device structure and J-V plots of the fabricated devices. The built-in potential (V$_{bi}$) increases after insertion of the Ba layer, as the work function of Ba (2.7 eV) is lower than Al (4.3 eV), which further assists faster sweep-out. Ba blocks the hole quite well even at high biases and serves good in increasing FF than other reported cathode interlayers. Ba as a CBL prevents the trap assisted shockley-read-hall (SRH) recombination at the interface, and enhancement in shunt resistance with the decrease in the series resistance is reported. The deposition of Ba shows improved performance due to modification of electrode work function. As the deposition of charge transport layers can modify the electrode work function and form the beneficial energy level alignment between active layer

and electrodes.[89–91] This resulted in an improved charge carrier collection probability, which further enhances FF and device performance.

2.3 Alkali metal compounds as CBL

Alkali metal fluorides have been widely used as CBL materials in OSCs. Among them, lithium fluoride (LiF) is one of the most commonly used material. The required optimum thickness of LiF is limited to less than 1 nm, as thick LiF layers are not favorable for efficient electron collection. In 2002, Brabec et al. [92] applied the thin interlayers of LiF, and it was incorporated in the MDMO-PPV: $PC_{61}BM$ active layer OSCs with Al cathode. As compared to the control device, the LiF led to a 20 % enhancement in PCE (~3.3 %). Figure 6(a) shows the J-V characteristics of the fabricated device at the different thicknesses of LiF. The LiF CBL resulted in dipole moment generation across the junction, owing to its orientation or chemical reactions occurring at interface, leading to charge transfer. This underlying mechanism is the probable cause of efficiency enhancement. [93] It has also been used as a composite CBL layer with C_{60} in P3HT:$PC_{70}BM$ blends for enhancement of PCE as well as helped in environment stability. In a similar way, other fluoride compounds of alkali metals such as sodium fluoride (NaF), cesium fluoride (CsF), and potassium fluoride (KF), etc., have been also explored as CBL materials, and a comparative study of the influence of LiF, NaF, and KF on the performance of OSCs has been investigated. The active layer used in all cases comprises of P3HT: $PC_{70}BM$ and Al as a cathode. Compared to LiF, NaF exhibited an improved PCE, FF, and an ultrathin layer thickness (<0.2 nm) (Figure 6b), suggesting NaF as a potential alternative for CBL. [94] In 2009, Jiang et al. [95] introduced the CsF as an interlayer, in the ITO/PEDOT: PSS/MEH-PPV: PCBM/CsF/Al device structure. The PCE of the device with Al/CsF cathode was higher (2.2 %) than Al/LiF cathode (PCE~ 1.40 %), under same illumination. The performance improvement with the Al/CsF

cathode was attributed to lower series resistance due to the dissociation of CsF on the deposition of Al, and generated a low work function Cs, thereby reducing the resistance between active layer and cathode interface. This further increases the interior electric field for efficient charge transport in the device. It was also proposed that the role of CsF is not only confined to dipole formation but also simultaneously modifies the polymer absorbing layer via diffusion. As per lattice energy of LiF and CsF, the CsF possesses a little higher tendency to dissociate. The enhancement of dissociation and diffussion of CsF into organic layer not only changes the interface but also bulk electric field structure. All these processes are strongly dependent on the type, nature, and thickness of the interlayer. Thus, CsF was found to have a similar effect to LiF even within much smaller layer widths. Hence, it was reported as an interesting alternative to LiF in OSCs and provides a comparatively higher lifetime. [95] [96] Recently, Mitul et al. [97] applied low (PDPP3T) and high (P3HT) bandgap donor polymers. The outcome of ITO/PEDOT: PSS/active layer/CsF/Al device structure, i.e., PCE of 2.83 % for 0.2 nm CsF than control (PCE~ 1.38 %) and 20 nm Ca (PCE~ 2.53 %) CBL, of P3HT/PCBM blend system. Figure 6(c-d) shows the device structure and corresponding J-V charectrisctics of the P3HT donor based devices. Furthermore, for the PDPP3T: $PC_{70}BM$ blend system, the device exhibited a PCE of 4.5 % of CsF interlayer with faster charge transport and low trap level.
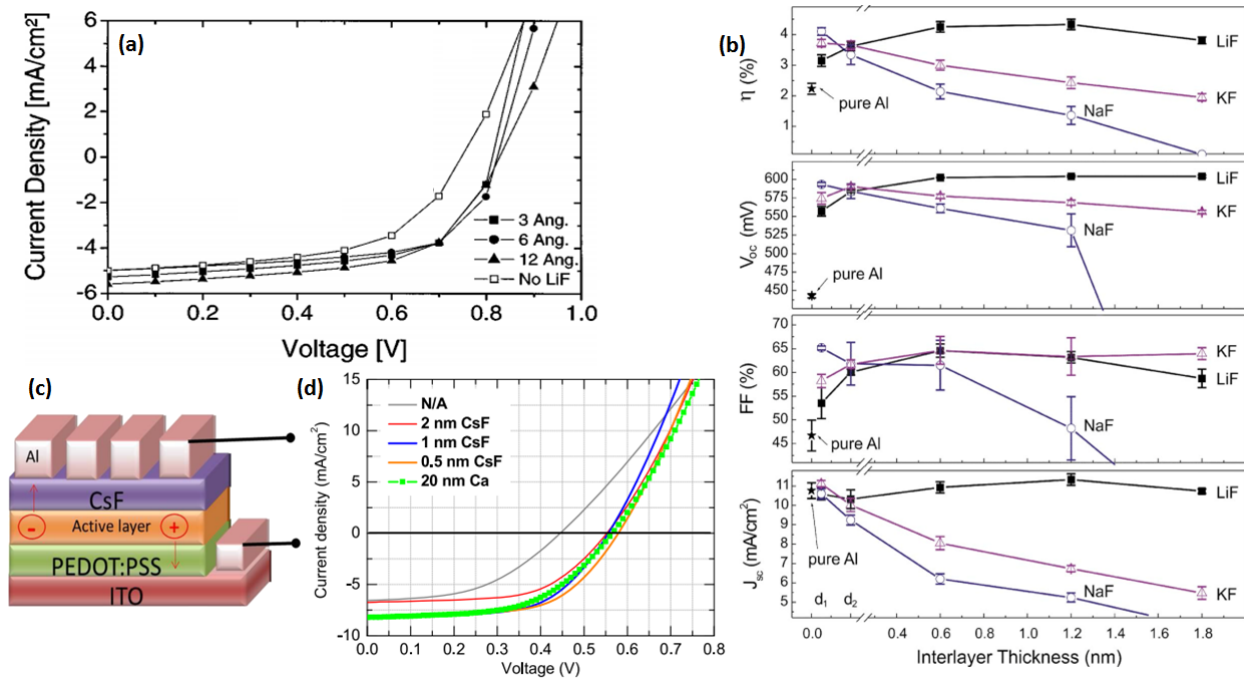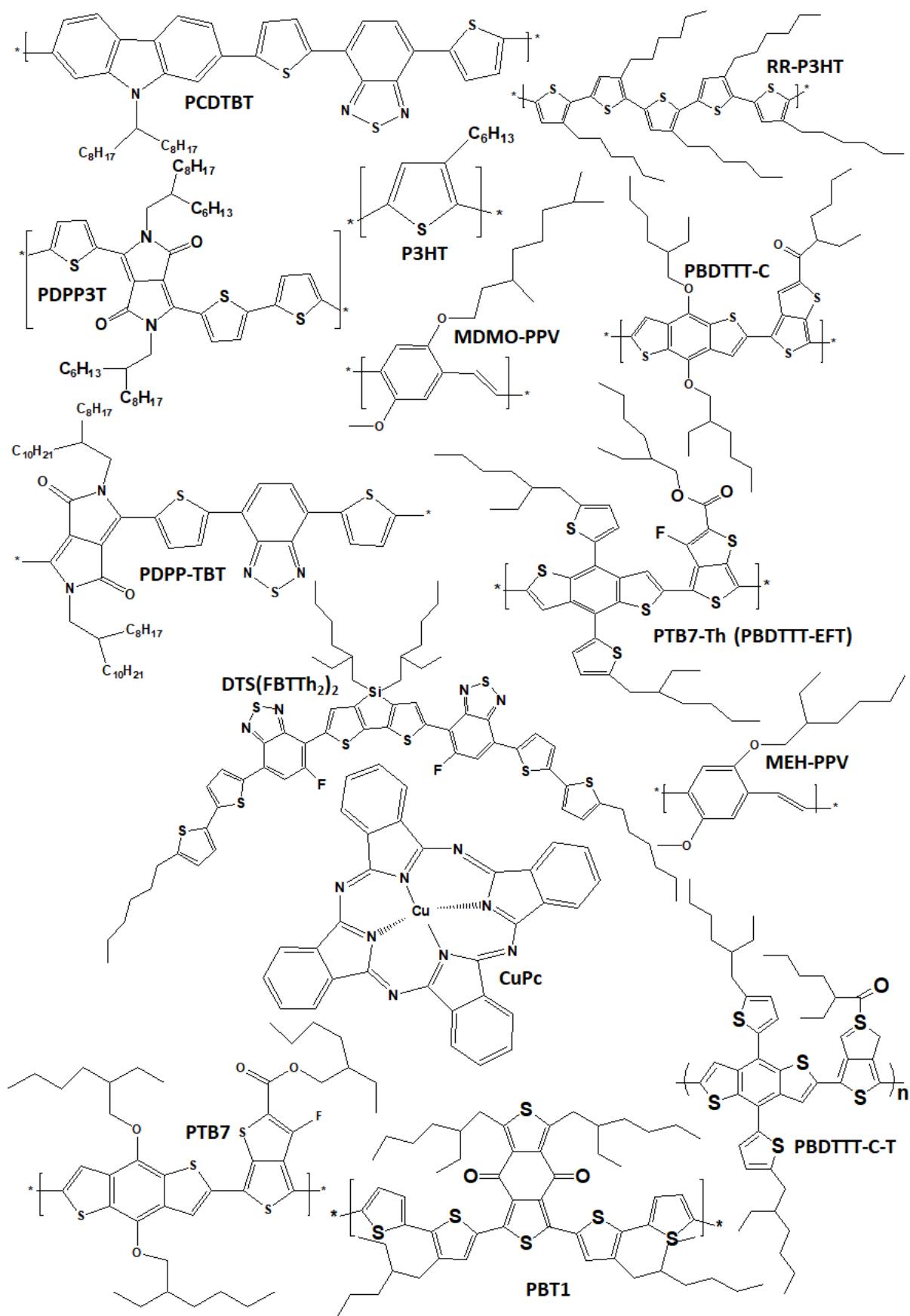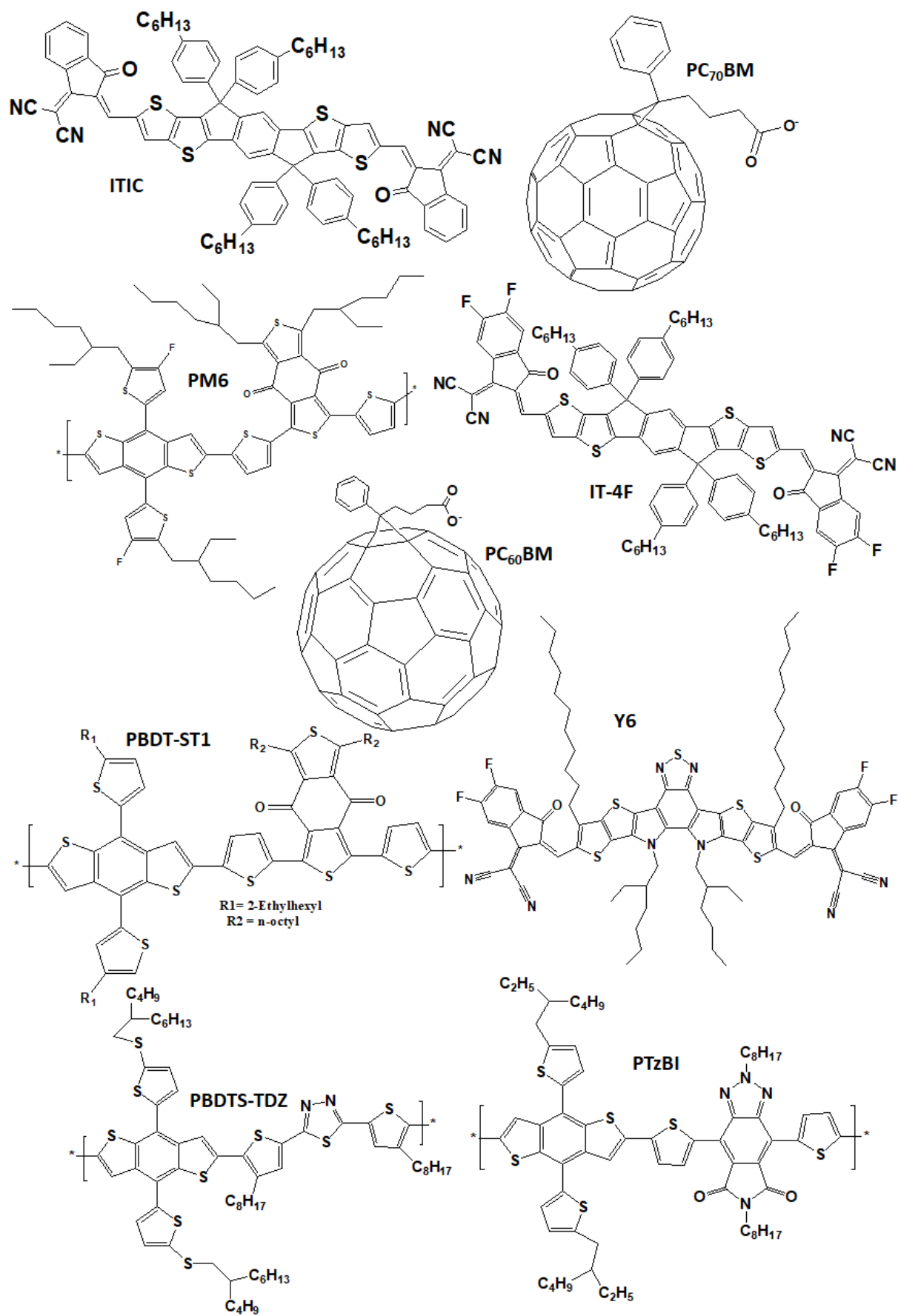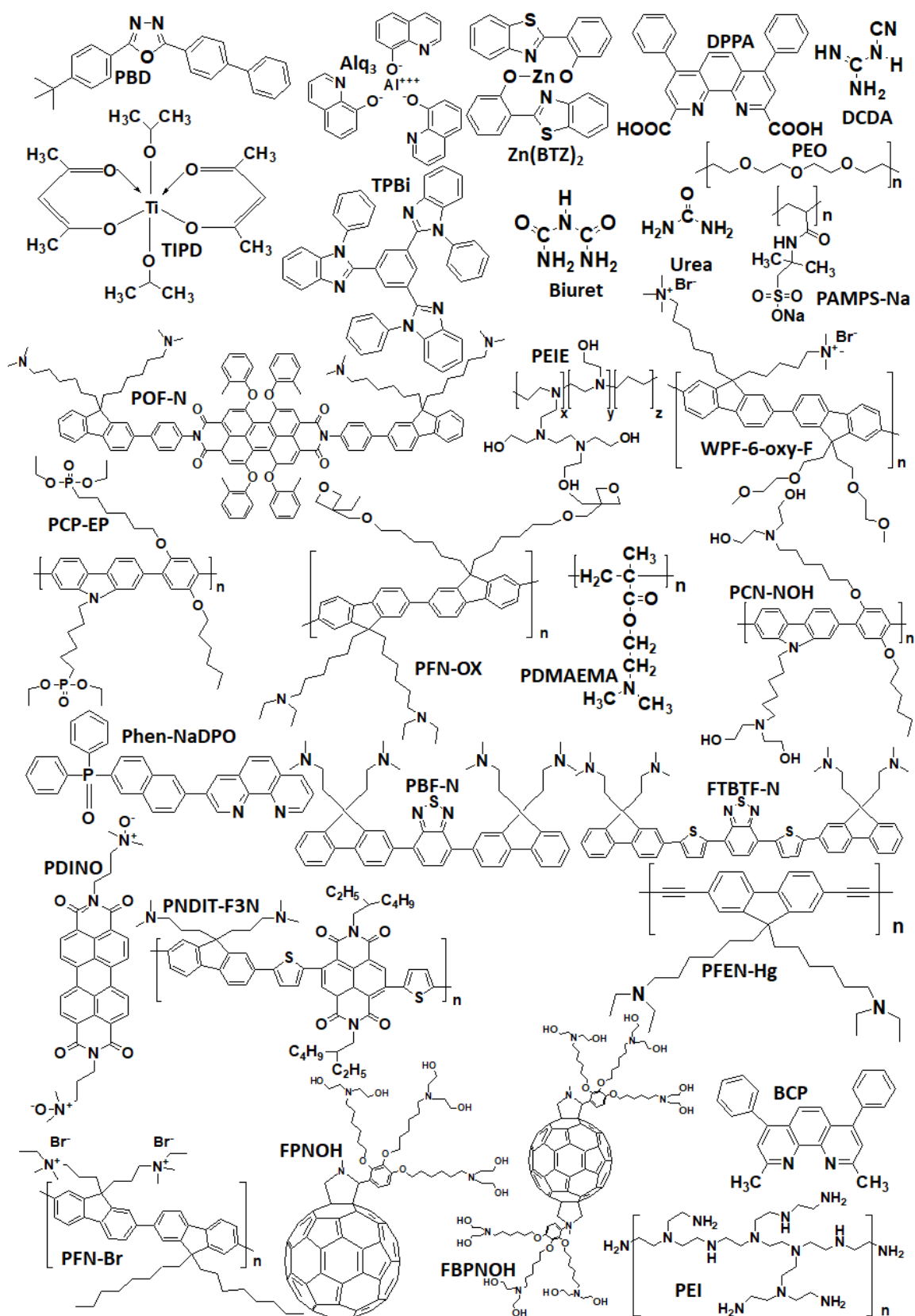
Figure (6): (a) J-V plot of MDMO-PPV: PCBM OSCs with a LiF/Al electrode at the various thickness of LiF (Å). Reproduced with permission from ref. [93]. Copyright © 2002, AIP Publishing. (b) The device performance parameters of P3HT: PCBM OSCs at different CBL of LiF, NaF, and KF with different thicknesses. Reproduced with permission from ref. [94]. Copyright © 2007, AIP Publishing. (c) Device structure using CsF interlayer and (d) J-V characteristics for optimization interlayer compared to Ca (CBL) in P3HT: PCBM blend system. Adapted from CC-BY open access publications (CC-BY license: 4.0) from ref. [97]. Copyright © 2018, Farzan et al.

PCDTBT

RR-P3HT

PDPP3T

P3HT

MDMO-PPV

PBDTTT-C

PDPP-TBT

PTB7-Th (PBDTTT-EFT)

DTS(FBTTh₂)₂

MEH-PPV

CuPc

PBDTTT-C-T

PTB7

PBT1

24

Scheme 1: Donor molecules molecular structures.

ITIC

PC$_{70}$BM

PM6

IT-4F

PC$_{60}$BM

Y6

PBDT-ST1

R1= 2-Ethylhexyl
R2 = n-octyl

PBDTS-TDZ

PTzBI

26

Scheme 2: Donor and acceptor molecules molecular structures

Scheme 3: Organic buffer layer molecules molecular structures.

2.4 Organic materials as CBL

Small-molecules

A diverse variety of organic materials including non-conjugated/conjugated polymers, small-molecules, and fullerene derivatives, have been explored as CBL in OSCs.[98–101] Out of these materials, small molecule-based CBL offers advantages owing to their well-defined molecular weight and easy purification process. Bathocuproine (BCP) is one the material whose film has been applied as CBL in various OSCs devices. Several groups have used a thin layer (1–10 nm) of BCP as a CBL. For instance, Chang et al. [102] investigated the effects of BCP on the P3HT: $PC_{61}BM$ blend system based OSCs, and found significant enhancements of V_{oc} (from 0.38 to 0.65 V) and FF (from 0.44 to 0.63) than control device. As a result, the PCE of the device was improved significantly from 1.63 to 4.11 % (at 2 nm BCP). The complete device parameters have been summarized in Table 3. Patil et al. [103] reported the BCP buffer layer in standard (Figure 7a) and inverted device structure of tetraphenyldibenzoperiflanthene (DBP) donor and fullerene (C_{70}) acceptor. The device with the BCP layer has shown enhancement of PCE of 4.06 % from 1.99 % of the control device. Figure 7 (b) shows the J-V characteristics for different thicknesses of BCP, and the performance parameters are also summarized in Table 3. Feng et al. [104] also applied the BCP as a CBL, in the ITO/PEDOT: PSS/ pentacene /P3HT:PCBM /BCP/Al device structure. The device with CBL exhibits the enhanced photovoltaic properties: J_{sc} is 6.28 mA/cm^2, V_{oc} is 0.6125 V, FF is 0.380, and PCE is 2.66 %, than control device in terms of V_{oc} of 0.4375 V, J_{sc} of 5.58 mA/cm^2, FF of 0.265 and PCE of 1.18 %. Recently, Kim et al. [105] demonstrated a thin pentacene layer as a CBL resulted in 50 % improvement in PCE ~ 3.1 % than control device (PCE~ 2%). The device structure was ITO/PEDOT: PSS/P3HT:

PC$_{61}$BM/CBL/Al. When 1 nm thick LiF was used, the corresponding PCE value of 2.7% was attained, in comparison to 3.1% with 1 nm thick pentacene. The 2-(4-biphenyl)5-(4-tert-butylphenyl) 1,3,4-oxidiazole (PBD), tris-8-hydroxy -quinolinato aluminum (Alq$_3$), and Bis[2-(2-benzothiazoly) phenolato] zinc(II) (Zn(BTZ)) small molecules were incorporated as a CBL in P3HT/PC$_{61}$BM blend system OSCs. [106] These were deposited by via thermal evaporation method. The control device has lower performance in terms of V$_{oc}$ of 0.42 V, J$_{sc}$ of 7.42 mA/cm^2, FF of 0.311, and PCE of 1.24 %. Whereas, the device with 0.5 nm PBD exhibits the enhanced properties: J$_{sc}$ is 7.61 mA/cm^2, V$_{oc}$ is 0.52 V, FF is 0.318, and PCE 1.60 %, enhanced by 30 % compared with control device. Li et al. [107] applied a solution-processable titanium chelate, titanium (diisopropoxide) bis(2,4-pentanedionate) (TIPD), as a CBL in MEH-PPV: PC$_{61}$BM OSCs. The introduction of a TIPD buffer layer reduced the interface resistance between the active layer and Al electrode, and consequently, the PCE reached 2.52 %, than control device (PCE~ 1.66 %).
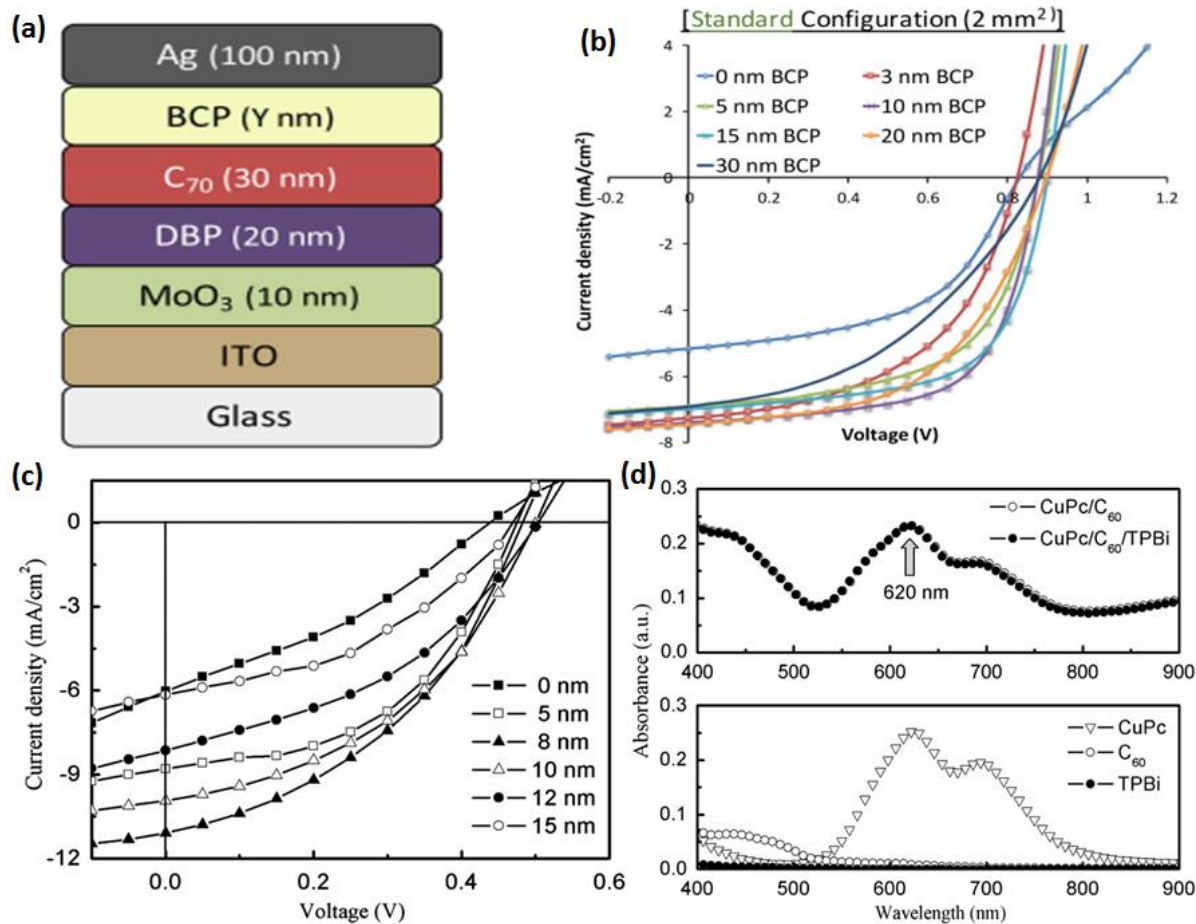
Figure (7): (a) Standard configuration of BCP buffer layer based OSCs device structure, (b) J-V plots at the different thickness of BCP in DBP: C_{70} active layer based OSCs. Adapted from CC-BY open access publications (CC-BY license: 4.0) from ref. [103] Copyright © 2018, Bhushan R. Patil et al. (c) J- V plots of CuPc: C_{60} blend system, and TPBi buffer layer based device, (d) Optical absorption spectra of CuPc: C_{60} with and without TPBi CBL layer. Reproduced with permission from ref. [108]. Copyright © 2010, Elsevier B.V. All rights reserved.

Table 3: Polymers CBL based convention devices performance parameters summary.

Device structure	Active layer	CBL	V_{oc} (V)	J_{sc} (mA/cm^2)	FF	PCE (%)	Ref.
ITO/MoO$_3$/Active layer/ CBL/Ag	DBP: C$_{70}$	-	0.81	4.95	0.49	1.99	[103]
		BCP (10 nm)	0.87	7.32	0.63	4.06	
ITO/PEDOT: PSS/ Active layer/ CBL/Al	P3HT: PCBM	-	0.38	9.54	0.44	1.63	[102]
		BCP (1 nm)	0.65	9.85	0.62	3.91	
		BCP (2 nm)	0.65	10.05	0.63	4.11	
		BCP (5 nm)	0.65	9.89	0.63	4.03	
		BCP (10 nm)	0.65	9.29	0.62	3.74	
		BCP (20 nm)	0.65	9.38	0.59	3.59	
		Alq$_3$ (2 nm)	0.59	10.09	0.53	3.18	
		Alq$_3$ (2 nm)/LiF (1.2 nm)	0.65	9.99	0.59	3.83	
		LiF (1.2 nm)	0.64	10.49	0.58	3.89	
ITO/PEDOT: PSS/Active layer/ CBL/Al	PTB7: PC$_{71}$BM	Ca	0.79	14.25	0.63	7.29	[109]
		PAMPS-Na	0.79	15.64	0.64	8.24	
	PTB7-Th: PC$_{71}$BM	Ca	0.80	14.57	0.69	8.32	
		PAMPS-Na	0.80	15.76	0.70	9.16	

	PBDT-ST1: PC$_{71}$BM	Ca	0.89	12.72	0.68	8.05	
		PAMPS-Na	0.89	13.62	0.73	9.09	
	p-DTS(FBTTh$_2$)$_2$: PC$_{71}$BM	Ca	0.80	13.41	0.65	7.30	
		PAMPS-Na	0.80	14.45	0.67	7.94	

Wang et al. [110], studied the 1,3,5-tris(2-N-phenylbenzimidazolyl) benzene (TPBi) as CBL, and introduced it in the ITO/PEDOT: PSS/ P3HT: PCBM/CBL/Al device structure. It exhibited PCE of 4.60 % than 2.14 % of control device. It is clear that the TPBi inserted between the photoactive layer and Al has improved the device performance. Yu et al. [108], also applied the TPBi CBL, in CuPc: C$_{60}$ blend system, and showed the remarkable enhancement of photovoltaic parameters such as J$_{sc}$ ~ 11.09 mA/cm^2, FF ~ 0.42, and delivered PCE up to 2.23 %, thereby showing more than 100 % improvement in comparison to the device without TPBi (PCE ~ 0.87). The measured J-V plots for different thickness of TPBi layer is shown in Figure (7c). Also, the improvement in J$_{sc}$ can correlate from the optical spectra of the active layer with and without TPBi, as shown in Figure (7d), which signifies the working of TPBi as an optical spacer and contributes as a buffer layer to enhance the overall absorption. Yang et al. [111] applied three amino-containing small-molecule—biuret, dicyandiamide (DCDA), and urea as a CBLs in ITO/PEDOT:PSS/P3HT: PC$_{61}$BM/CBL/Al, resulting in improved PCE of 3.84 %, 4.25 %, and 4.39 % for biuret, DCDA, and urea, which were enhanced by ~15 %, ~27 %, and ~31 %, respectively, compared to control device. The efficiency enhancement was due to the formation of a dipole layer between the P3HT: PC$_{61}$BM active layer and the Al electrode, which decreased effectively, the energy level offset between the work function of Al and the LUMO level of the

PC$_{61}$BM acceptor, resulting in improved electron extraction. Yang et al. [112] introduced an amphiphilic surfactant oleamide as a novel CBL and it was doped into P3HT: PCBM blend. After coating, it migrated onto the P3HT: PC$_{61}$BM active layer surface via self-assembly, and formed the oleamide self-assembled CBL layer. It resulted in a significant PCE enhancement by ~28 %, from 3.09 to 3.94%. The improvement was primarily due to the increase of J$_{sc}$, V$_{oc}$ and FF, from 10.21 to 10.29 mA/cm^2, 0.62 to 0.64 V, and 0.49 to 0.60, respectively. Initially, there was a significant energy level offset (0.3 eV) between the LUMO level of PCBM (4.0 eV) and the WF of Al (4.3 eV), and it resulted into an unfavorable electron extraction. After doping with oleamide, there is a formation of an oleamide interfacial dipole layer that could lower the work function of Al. Thus, it lowered the energy level offset between LUMO level of PCBM and the Al work function, and consequently, facilitated the electron extraction.

Polymers

Cai et al. [109] designed and synthesized the non-conjugated novel polymer namely PAMPS-Na. It was soluble in polar solvents, including water, methanol, and ethanol, and thus was suggested as a potential solution-processable CBL for OSCs. Additionally, PAMPS-Na could reduce the work-function of Al electrode. To establish the suitability of PAMPS-Na as a CBL, a few devices were fabricated using a variety of different donor molecules. The energy level diagram is shown in Figure 8 (a). In this structure, the PAMPS-Na-modified the Al electrode and its work function (Figure 8b) has changed from -4.30 eV to -3.51 eV, which was thought to be favourable for electron extraction. The device with PAMPS-Na/Al showed improvement in photovoltaic performance with higher J$_{sc}$ in comparison to Ca/Al-based. Figure 8 (c-d) has shown the J-V characteristic of polymer (PTB7) and small molecule (p-DTS(FBTTh$_2$)$_2$) donors based, and with and without PMAMPS-Na CBL devices. The device performance parameters are summarized in

Table 3. Four different donor molecules (PTB7, PTB7-Th, PBDT-ST1, p-DTS(FBTTh$_2$)$_2$) were studied and the enhancement was mainly observed in the J$_{sc}$ as well as FF. For PTB7: PC$_{71}$BM, PTB7-Th: PC$_{71}$BM, PBDT-ST1: PC$_{71}$BM, and p-DTS (FBTTh$_2$)$_2$: PC$_{71}$BM blend systems, the PCE were 8.24, 9.16, 9.09, and 7.94 %, than control device (Ca/Al), 7.29, 8.32, 8.05, and 7.30 %, respectively. Moreover, the stability of PMAMPS-Na CBL based devices has been studied and it is under ambient condition observed for 30 days. It showed an improvement than the devices with Ca/Al. Thus the study marked the promising nature of PAMPS-Na as CBL for enhanced efficiency and stability. The device with PAMPS-Na/Al retained the 77 % PCE of its intial value as compared to Ca/Al, which had 66 % after 30 days in ambient condition. The PAMPS-Na is considered to be a potentially efficient and cost-effective CBL for use in OSCs.
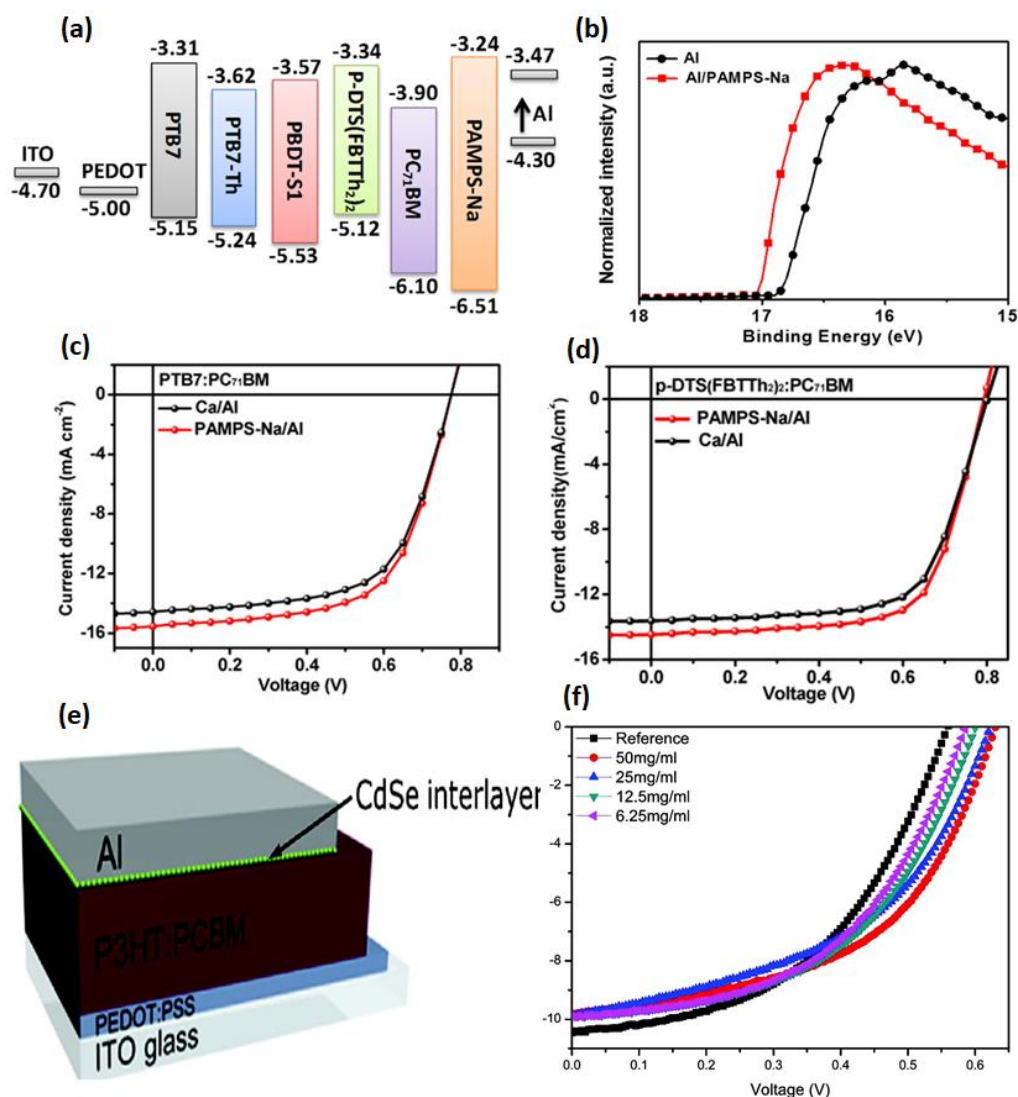
Figure (8): (a) Energy level diagram of donor molecules with PAMPS-Na CBL, (b) Ultraviolet photoelectron spectroscopy (UPS) measurement of Al, and Al/PAMPS-Na electrode. J-V characteristics of (c) polymer donor blend PTB7: $PC_{71}BM$, and (d) small molecules p-DTS(FBTTh$_2$)$_2$: $PC_{71}BM$ blend based OSCs, with and without PAMPS-Na layer. Reproduced with permission from ref. [109]. Copyright © 2018, American Chemical Society. (e) Device structure of CdSe QDs interlayer OSCs, (f) J-V characteristic of OSCs at different concentration of CdSe interlayer. Reproduced with permission from ref. [113]. Copyright © 2012, American Chemical Society.

2.5 Quantum dots (QDs) as CBL

The quantum dots were previously well-reported for solar cell fabrication because of their tunable optical and electrical properties. [114,115] Jeon et al. [113] introduced a cadmium selenide (CdSe) QDs layer, deposited by a stamping transfer process instead of a direct spin coating process on top of the P3HT: PCBM layer. The QDs film prepared on SAMs-treated Si wafer, were then transferred on top of the active layer. The device (Figure 8e) performance parameters of QDs interlayers-based devices with different concentration of CdSe QDs are summarized in Table 4. The reference device showed V_{oc}, J_{sc} and FF of 0.57 V, 10.4 mA/cm^2 and 0.40, respectively, and delivered PCE of 2.39 %. For QDs device, its concentration was taken at 6.25, 12.5, 25, 50 mg/ml, and the optimized OSCs performance was delivered at 58 mg/ml (Figure 8f). The device parameters were; V_{oc} = 0.63 V, J_{sc} = 9.9 mA/cm^2, FF= 0.49, and PCE = 3.08 %.

Table 4: Quantum dots CBL based conventional device performance summary.

Device structure	Active layer	CBL	V_{oc} (V)	J_{sc} (mA/cm^2)	FF	PCE (%)	Ref.
ITO/ PEDOT: PSS/ Active layer/CBL/ Al	P3HT: PCBM	-	0.57	10.4	0.40	2.39	[113]
		CdSe, 50 mg/mL	0.63	9.90	0.49	3.08	
		CdSe, 25 mg/mL	0.62	9.90	0.47	2.88	
		CdSe, 12.5 mg/mL	0.61	9.90	0.45	2.72	

		CdSe, 6.25 mg/mL	0.59	9.90	0.44	2.66	

Although efficiency up to 15.7 % in conventional OSCs have been achieved, still the realization of the long-term stable device remains a crucial challenge owing to the high susceptibility of low WF metals to atmospheric moisture or oxygen in the conventional OSCs. This hinders the commercial applications of the devices. [87,116] Moreover, in the conventional architecture OSCs, the PEDOT: PSS layer etches the ITO coating, thereby affecting the overall device performance. [117,118] This has led to the emergence of inverted organic solar cells (i-OSCs), where the charge carrier's collection is reversed. The details of CBL materials explored and used in i-OSCs are given below.

3. Materials for cathode buffer layer: inverted architecture

3.1 Oxide, acetylacetonate and carbonates as CBL

Oxides

Titanium dioxide (TiO$_2$)

Oxides are one of the most common choices as CBL owing to their tunable optical and electrical properties. These led to substantial increase in the device stability in air and under light. In recent years, TiO$_2$ has been used as CBL in a variety of i-OSCs. [119–121] In 2011, Kang et al. [122] represented how the crystallinity of the electron transport layer can dramatically influence the transient characteristics of OSCs. They employed an inverted device structure (ITO/TiOx/P3HT: PCBM/PEDOT: PSS/Ag) using 10 and 20 nm thickness of TiO$_x$, prepared by atomic layer

deposition as a CBL. The X-ray diffraction pattern indicated that 10 nm thick TiO_x film has amorphous behavior as compared to 20 nm. The device with amorphous phase TiO_x reported an enhancement in device parameters on continuous light exposure in the ambient conditions, probably due to the filling of shallow electron traps present in amorphous phase TiO_x (10 nm) upon illumination. In contrast, the device parameters of the crystalline phase TiO_x (20 nm) based device, showed a negligible enhancement on continuous illumination. The 20 nm TiO_x exhibit parameters as J_{sc} = 9.24 mA/cm^2, V_{oc} = 0.59 V, FF= 0.56 , and PCE= 3.09 % which are higher than 10 nm thick TiO_x device (J_{sc} = 8.65 mA/cm^2, V_{oc} = 0.54 V, FF= 0.40, and PCE= 1.89 %). The device performance parameters have improved in the case of 20 nm TiO_x. The atomic layer deposition deposition of TiO_2 interface has been also reported by Lin et al. [120] in P3HT: PCBM blend system. They reported the light soaking effect in the TiO_x based device (Figure 9b). Figure 9 (a) shows the favourable energy level alignment of TiO_x with ITO and active layer. In the optimized case, the device after light soaking (for 5 minutes) presented PCE improvement from 1.33 to 3.31 %, which was double of its initial value. The doping of reduced graphene oxide (RGO) has been also investigated with TiO_x, called RGO/TiO_x composite films and it was explored as CBL [123]. Zhang et al. [124] introduced the RGO/TiO_x composite, an enhancement in the J_{sc} of 9.85 mA/cm^2 and PCE of 3.82 % was achieved. The obtained PCE has improved significantly in comparison to the control device (PCE~ 3.03). It was concluded that the enhancement is probably due to improved electron transport properties of the RGO/TiOx based CBL. Yang et al. [125] incorporated the TiO_x with polyethylenimine (PEI) as a CBL and the resultant PCE improved up to 9 % as compared to the control device (7.38 %) or with PEI (7.00 %). The TiO_x/PEI combination helped to reduce the series resistance and boosted the electron extraction at the interface of the cathode. Furthermore, the PEI layer minimizes the contact

resistance between TiO_x and the $PTB7:PC_{71}BM$ layer, as reported via electrical impedance spectroscopy. Moreover, the PEI coating above the TiO_x reduced the work function of $ITO/TiO_x/PEI$ from 4.42 (ITO/TiO_x) to 4.20 eV. The photo-generation of charge carriers was enhanced after using TiO_x/PEI CBL layer.
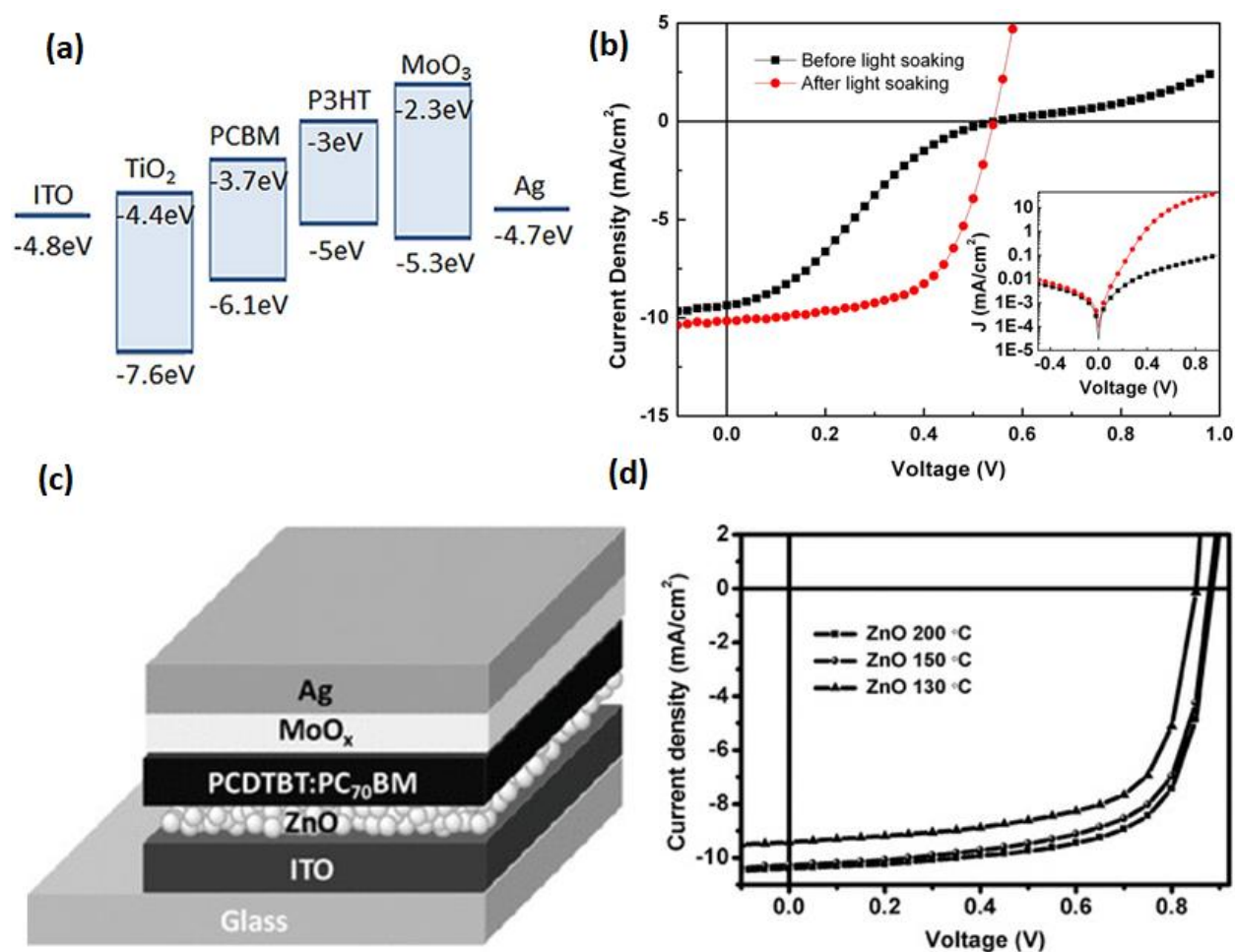

Figure (9): (a) Energy level diagram of TiO_2 CBL based device, (b) J-V characteristics of devices, and employed TiO_2 layer shown light soaking effect (inset dark J-V characteristics). Reproduced with permission from ref. [120]. Copyright © 2013, American Chemical Society (c) ZnO interface layer based inverted device structure, and (d) J-V curve of PCDTBT: $PC_{70}BM$

device at different annealing temperatures of ZnO buffer layer. Reproduce with permission from ref. [126]. Copyright © 2011 WILEY-VCH Verlag GmbH & Co. KGaA, Weinheim.

The TiO_x modified with a thin layer of Al was incorporated as CBL in an i-OSCs based on the P3HT: PCBM active layer. The role of the thin Al layer was in improving the surface properties of TiO_x and minimizing the work-function of it, and it further enhanced the built-in voltage and facilitated the electron extraction. All these resulted in an efficient device with PCE of 3.6 %, V_{oc} of 0.60 V, J_{sc} of 9.13 mA/cm^2, and FF of 0.66. The light soaking problem was eliminated compared to the TiO_x CBL device [66]. The TiO_x conductivity is sensitive to light illumination, as this can excite electrons from valence band to the conduction band, and such early excited electrons must fill the shallow electron traps of TiO_x conduction band. Thus, in TiO_x, the photoconductivity (on light exposure) increases initially and afterward saturates after filling of all shallow traps. They hence attributed an improvement in the device behavior to the filling of the shallow electron traps in the TiO_x and also it can be concluded that the photoconductivity of the TiO_x increases with a decrease in the serial resistance in the inverted device. [127] However, the organic/inorganic interface of polymer and TiO_2 has shown the poor contact and resulted in the loss of J_{sc} as well as FF. To improve these organic/inorganic contacts, an interlayer has been introduced between TiO_2 and active layer, and it is termed as interface passivation. Li et al. [128] introduced the series of conducting polyfluorenes (PF) molecules, namely PDF, PDFBT, and PFTBT as a passivating materials for TiO_2 layer that boosted the charge extraction of combined CBL layer. The PCE has shown an enhancement from 5.72 % to 6.66, 6.72, and 7.97 % for PFTBT, PDF, and PDFBT molecules, respectively. Furthermore, an improvement has been seen in all the device parameters (V_{oc}, Jsc, FF). The utilization of passivation technique could improve

the energy level alignment and provide effective interfacial adhesion between CBL and active layer.

Zinc oxide (ZnO)

In recent years, CBLs comprising of pristine ZnO, doped-ZnO, and ZnO-based composites, as well as the surface modified ZnO-based layers have been used by several research groups for enhancing the device parameters of inverted architecture OSCs. The ZnO is one of the potential choices as CBL in i-OSCs owing to its enhanced electron mobility, high transparency, easy synthesis, and high stability. Takahashi et al. [129] used the electrodeposition method to insert the ZnO into the OSCs, and they were amazed by the remarkable performance enhancement. The standard device ITO/CBL/PV/MEH-PPV/PEDOT: PSS/Au, (where PV: bisbenzimidazo [2,1-a:2′,1'-a'] antra [2,1,9-def:6,5,10-d'e'f'] diisoquinoline-6,11-dione), had high PCE of 1.24 % than control device (0.21 %). A sol-gel derived ZnO CBL was reported by Kyaw et al. [118] in the i-OSCs device. By modifying the precursor solution concentration from 0.75 to 0.1 M, the optical transmittance of ZnO film can be tuned from 75 to 95 %. The optimized device gains the PCE up to 3.09 % at the 0.1 M ZnO precursor solution. Table 5 has summarized the device results under illumination at different concentrations of ZnO. In i-OSCs, the thickness of ZnO is in nanometers to provide conductivity with less series resistance. [130] The low thickness of ZnO CBL based devices suffer from low mechanical robustness and device goes under degradation due to chemical or physical reactions between the active layer and the electrode. To overcome this issue, researchers have come up with solutions such as doping of a new materials into ZnO. The doping not only improves its optical and electrical properties simultaneously, but also helps in resolving the thickness related issue of ZnO, and also make improvement in its conductivity.

There are several reports in which researchers have used doped ZnO as CBL, and they have achieved improvement in device parameters of i-OSCs. [131–134] Commonly used dopants are I, II, and III group elements. Besides these, transition metal ions and rare-earth elements are also doped in ZnO to improve its optical properties, thereby contributing in PCE enhancement. In 2016, a luminescent ZnO-Na (L-ZnO) CBL has been introduced in the small-molecule (p-DTS(FBTTh$_2$)$_2$) donors based OSCs with their improved efficiency and stability in comparison to control device. [135] The L-ZnO CBL also worked to absorbs incoming ultraviolet (UV) light and converted it into visible light, and this phenomenon is called as down-conversion. The emission of the L-ZnO layer overlaps significantly with the absorption of p-DTS(FBTTh$_2$)$_2$, leading to an enhanced absorption of p-DTS(FBTTh$_2$)$_2$ and thus improved the PCE as well as stability under UV irradiation of the resultant device. Our group [136] also reported the europium (Eu) and aluminum (Al) doped ZnO CBL, and is denoted as ZnO: Al, Eu. It worked as dual-functional layer (down conversion as well as ETL), and the device (ITO/CBL/PCDTBT: PC$_{71}$BM/MoO$_3$/Ag) delivered the PCE of 6.9 % with Eu and Al doped CBL than the control device (PCE~ 5.9 %). Sun et al. [126] reported the solution processable sol-gel derived ZnO buffer for an inverted device structure (Figure 9c) that significantly enhanced the device performance. The ZnO could be processed by spin coating even at low temperatures, and its long-term stability made it attractive for future applications. The annealing of ZnO helped the film in increasing its crystallinity, and influencing the device parameters. The J-V characteristics of the devices at different annealing temperatures (130, 150, 200 ºC) of the ZnO buffer layer is shown in Figure (9d). The optimized result was obtained at 200 ºC anealing temprature, and device delivered PCE up to 6.33 % as compared to PCE of 5.36 % for 130 ºC ZnO annealing temperature. The ZnO, owing to its easy processing and stability, has been popularly applied as

CBL with different donor and acceptor molecules. [137–142] The solution proccessd ZnO has also shown the surface defects, and introduced the trap states as charge carrier recombination centre. To solve these issues, the further treatment of ZnO has been suggested and it is called passivation of ZnO surface. Pandi et al. [143] introduced the reduced graphene oxide (rGN) sheet and it improved the charge transport properties by reducing the surface defects. Similar mechanism has been reported by using triethanolamine and indum (In).[144][145] Jiang et al.[144] suggested that with triethanolamine, the passivated ZnO film has reduced the trap density by two orders, improved the charge carrier recombination time by three orders and it helped to increase the electron mobility as well as overall device performance.

Niobium pentoxide (Nb$_2$O$_5$)

The role of wide bandgap oxide thin layer in i-OSCs was investigated by Wiranwetchayan et al. [146] by employing a thin film (10 nm) of TiO$_2$ and Nb$_2$O$_5$ as CBL in the FTO/CBL/P3HT: PCBM/PEDOT: PSS/Ag device structure. The use of the TiO$_2$ buffer layer leads to PCE of 2.8 % than for Nb$_2$O$_5$ (2.7 %). Moreover, the performance of OSCs at different thickness of buffer layer has also been investigated and it suggests that Nb$_2$O$_5$ is more sentive to its thickness than TiO$_2$. At low thickness Nb$_2$O$_5$ based devices PCE decreased to even zero. Whereas for TiO$_2$ device it decreased from 2.8 to 2.3 %. The Nb$_2$O$_5$ conduction band is higher than the LUMO level of PCBM acceptor. Figure 10 (a-b) shows the corresponding J-V curve under illumination, and the device energy level diagram. The experiments concluded that there exists a tunneling mechanism for the electron transport from the PCBM to cathode over the oxide film, thereby neglecting the occurrence of electron diffusion mechanism arising due to energy or concentration gradient.
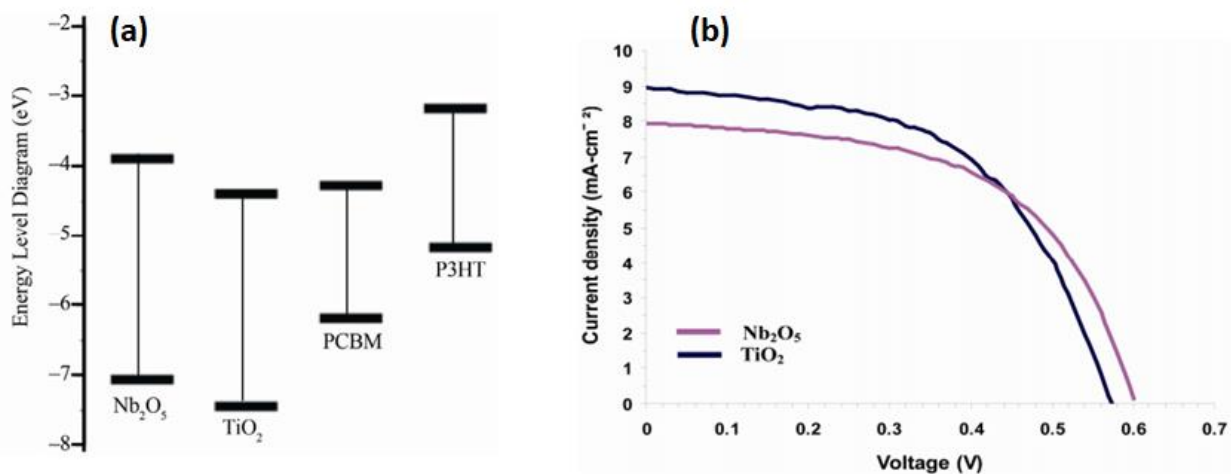
Figure (10): (a) Energy level diagram of Nb_2O_5, TiO_2, PCBM and P3HT layers, and (b) J-V plot of FTO/TiO_2 or Nb_2O_5/P3HT: PCBM/PEDOT:PSS/Ag device, under illumination. adapted from CC-BY open access publications (CC-BY license:4.0) from ref. [146]. Copyright © 2011, O. Wiranwetchayan et al.; SciRes.

Aluminium oxide (Al_2O_3)

An ultrathin (1 nm) Al_2O_3 layer was employed as CBL in i-OSCs by Zhou et al. [147]. The Al_2O_3 layer was deposited by an atomic layer deposition method, on top of ITO, which led to reduction in the work function of ITO, thereby acted as a cathode. The work function of deposited Al_2O_3 buffer layer depends on the thickness of the film. The device based on P3HT: $PC_{60}BM$ blend system has yielded a FF of 0.64 and a PCE of about 2.8 %, under 100 mW/cm^2 illumination. The device with Al_2O_3 showed a kink in the J–V curves measured under illumination. The kinks could be removed by UV exposure or electrical bias and was reappeared upon air exposure. This fully reversible phenomenon is tentatively due to the desorption and adsorption of oxygen. The desorption of oxygen in the Al_2O_3 layer is induced by holes that are either photogenerated by UV

illumination or electrically injected. After removal of the kinks, the solar cells exhibited a PCE of 2.8 %. The solution-processable Al_2O_3 was used as CBL by Peng et al.[64] for i-OSCs with P3HT: PCBM blend system. The device performance was studied at different annealing temperatures of Al_2O_3, and optimal result was obtained at 150 ºC (PCE~ 3.6 %) as compared to 300 ºC (PCE~ 2.4 %). Since Al_2O_3 is an insulating material, the optimized thickness of ~2 nm was used to minimize the series resistance. Its AFM images suggested the Al_2O_3 coated ITO film roughness (root mean square (RMS)~2.5 nm) was less as compared to bare ITO (RMS~ 3.6 nm) surface. The Al_2O_3 precursor solution was spin-coated at 5000 rpm for 40 s and annealed at 150 ºC, and for control device, the thermally evaporated the aluminum layer was used, which is denoted as e-Al_2O_3. It was deposited up to ~2 nm and treated in UV-O_3 chamber. The spin-coated Al_2O_3 device has shown enhanced performance as compared to e-Al_2O_3 and ZnO based devices. The device performance parameters are summarized in Table 5. The Al_2O_3 films have also been reported as an electron transport layer in conjugation with other materials like SiO_2 and ZnO as CBL. [148,149]

Zirconium and aluminium acetylacetonate

Among the CBL materials, zirconium acetylacetonate (ZrAcac) and Aluminum(III) acetylacetonate (Al(acac)$_3$) have been also studied in i-OSCs as CBL layer. Fan et al. [150] introduced the ZrAcac as CBL, in the device structure of ITO/ZrAcac/PTB7-Th: $PC_{71}BM$/MoO_3/Al. The optimal device delivered the PCE up to 9.2%, with J_{sc}, FF, and V_{oc}, of 17.74 mA/cm^2 , 0.66, 0.78 V, respectively. Moreover, the selection of solvent for ZrAcac can improve the device performance. Thus the chloroform-processed ZrAcac has shown the remarkable performance (PCE~ 9.21%) than methanol processed (PCE~ 8.46%) ZrAcac. The

introduction of ZrAcac has been also reported on top of ZnO as an auxiliary buffer layer in the ITO/ZnO/ ZrAcac/ active layer/MoO$_3$/electrode device structure for different active layers.[151] By using ZrAcac, the PCE has been improved from 7.60 to 8.15 %, 8.46 to 9.37 %, and 9.89 to 11.18% for PTB7-Th: PC$_{71}$BM, PBDB-T: ITIC and PBDB-TF: IT-4F blend system devices, respectively than their control devices. An improvement has been observed in all the three devices performance parameters such as V$_{oc}$, J$_{sc}$, and FF. It is suggested that a thin ZrAcac layer could reduce the charge transport resistance by minimizing the trap states. In acetylacetonate family, the aluminum (III) acetylacetonate (Al(acac)$_3$) also has been introduced in OSCs as CBL. However, it is well studied in perovskite solar cells that the doping in the perovskite precursor solution helps in reduction of the microstrain in the polycrystalline perovskite film. [152,153]

Cesium carbonates

The effect of cesium carbonate has been investigated as an interlayer in i-OSCs as well as in the LED devices, via various research groups. [154] In 2006, Li et al. [155] introduced Cs$_2$CO$_3$ as CBL with V$_2$O$_5$ as HTL for the enhancement of i-OSCs performance. The Cs$_2$CO$_3$ (1 nm) was thermally evaporated to modify the ITO work function, in the device structure of ITO/Cs$_2$CO$_3$/P3HT: PCBM/V$_2$O$_5$/Al. The control device (ITO/blend/Al) was observed with J$_{sc}$, V$_{oc}$, FF, and PCE of 4.75 mA/cm^2, 0.22 V, 0.28.5 and 0.23 %, respectively. After modification of ITO by a thermally evaporated layer of Cs$_2$CO$_3$ (1 nm), it helps to enhance the device parameters such as J$_{sc}$, V$_{oc}$. FF and PCE which were found to be 8.42 mA/cm^2, 0.56 V, 0.62, and 2.25 %, respectively. For solution-processable Cs$_2$CO$_3$, the device results are low as compared to thermally evaporated Cs$_2$CO$_3$ interlayer. Liao et al. [156] reported the Cs$_2$CO$_3$ interlayer thermal annealing effect on i-OSCs device. They have shown the Cs$_2$CO$_3$ WF modification from 3.45 to 3.06 eV by buffer layer annealing technique, which helped to enhance the V$_{oc}$ of the cells. The

device structure was ITO/Cs_2CO_3/RR-P3HT: PCBM/V_2O_5/Al. The devices were studied at no annealing (N/A) and 70, 120, 150, 170, and 200 ^{o}C annealing temperature. The N/A device has shown the V_{oc}. J_{sc}, FF, and PCE of 0.550 V, 7.61 mA/cm^2, 0.55, and 2.31%, respectively. In annealed CBL, the V_{oc} was enhanced, at 70°C (0.565 V), 120°C (0.580 V), 150°C (0.590 V), 170°C (0.582 V), and 200°C (0.584 V). The optimized result was received at 150 ^{o}C annealing temperature, and showed PCE up to 4.19 %. The Cs_2CO_3 interlayer was also reported by Kim et al. [157] and it was doped with ZnO. The CBL solution was prepared by mixing ZnO and Cs_2CO_3 at the five different ratios of 1:1, 1:2, 1:3, 2:1, and 3:1. Inverted ITO/ (ZnO or ZnO/Cs_2CO_3)/P3HT: PCBM/PEDOT: PSS/Al device structure was used for the experiment. The measured J-V characteristics are presented in Figure (11a) in which devices A and B belong to ZnO, and ZnO/Cs_2CO_3 devices, respectively. The device A and B have PCE of 2.89 and 3.12 %, respectively. The main improvement was observed in J_{sc} and FF, and the V_{oc} remained unchanged due to interface modification, and hence the charge collection gets enhanced, with reduced recombination. The concept of dual electrons transport layers (layer by layer deposition of two CBL) was introduced by Tran et al. [158]. They introduced Cs_2CO_3 and SnO_2 as solution-processable CBL for enhancing the device performance parameters in i-OSCs. The SnO_2 is a wide-bandgap (3.6 eV) and nontoxic material, and having good optical and electrical properties. Generally dual CBL layer is used to modifiy the electrode morphology as well as work function. In this case an author claimed the reduction of surface roughness of ITO/SnO_2 from 0.84 to 0.78 nm. Moreover, after coating Cs_2CO_3 (ITO/SnO_2/Cs_2CO_3), the work function also declined from -4.34 to -4.16 eV (for 0.5 mg/ml Cs_2CO_3), respectively. The dual CBL step by step deposition process is shown in Figure (11c). Firstly, the SnO_2 precursor solution was spin-coated (3000 rpm, 40 s) and was followed by annealing at 180 ^{o}C for one hour in ambient condition and after

cooling it down, the Cs_2CO_3 was spin-coated and was further dried at 100 °C. The final CBL film was SnO_2/Cs_2CO_3. The Cs_2CO_3 films were coated from three different precursor concentrations of 0.5, 1.5, and 3.5 mg/ml. The measured transmission spectra of SnO_2 and SnO_2/Cs_2CO_3 films on glass substrates are shown in Figure (11b), which indicates that the dual CBL layer has maintained the good transparency in visible region. The measured J-V under illumination of 100 mW/cm^2 are mentioned in Figure (11e). The device performance for SnO_2 CBL based device were, J_{sc} ~10.16 mA/cm^2, V_{oc} ~0.55 V, FF ~0.47, and PCE 2.68 %. After coating the Cs_2CO_3 layer on top of the SnO_2, the device parameters were changed and highest performance was achieved for the 0.5 mg/ml concentration of Cs_2CO_3. The FF and V_{oc} were the improved key parameters after dual CBL layer coating. The PCE were 3.69, 3.50, and 2.24 %, for 0.5, 1.5, 3.5 mg/ml concentration of Cs_2CO_3 interlayer. It reveals that the current density of the electron-only devices dropped drastically with increase in the concentration of Cs_2CO_3 from 0.5 to 3.5 mg/ml (Figure 11d). The study suggested a negative effect on SnO_2 with an overdue amount of Cs_2CO_3 (1.5 or 3.5 mg/ml).
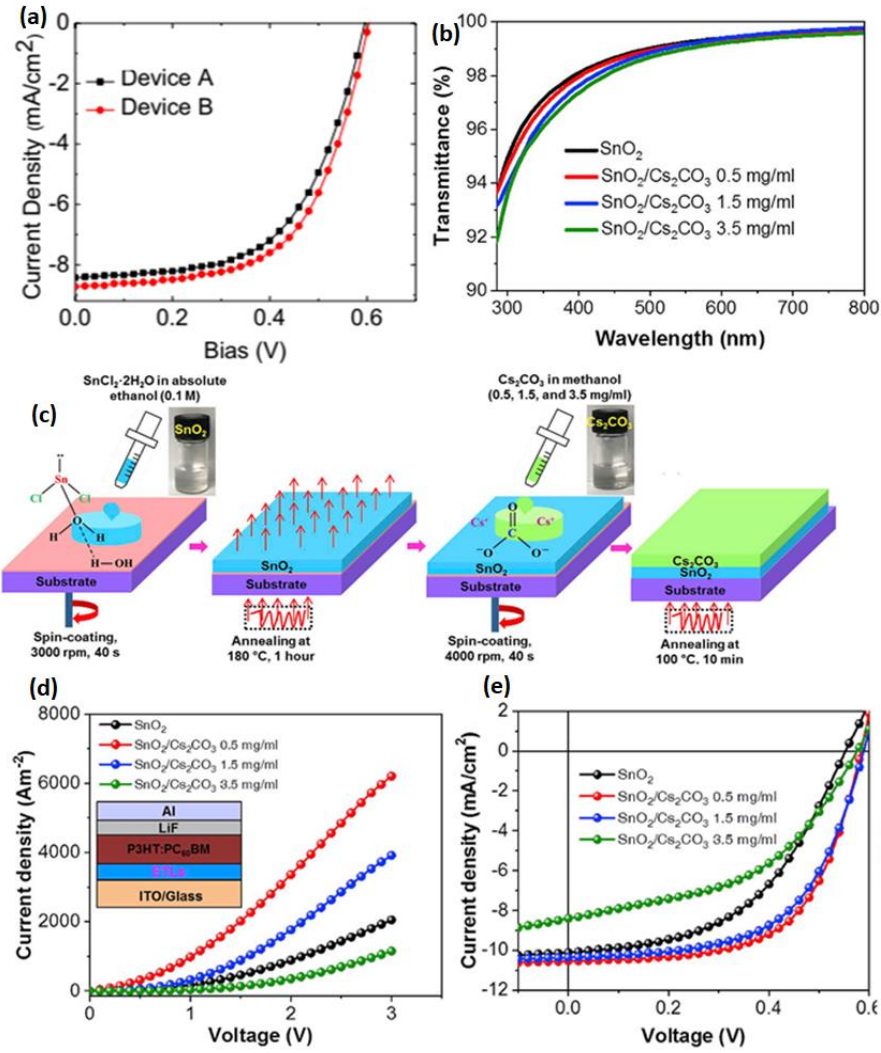
Figure (11): (a) J-V plot of P3HT: PCBM inverted device of A (ZnO) and B (ZnO/Cs$_2$CO$_3$) CBL. Adapted from CC-BY open access publications (CC-BY license: 4.0) from ref. [157]. Copyright © 2014, Kim et al.; licensee Springer. (b) Transmittance spectra of SnO$_2$/Cs$_2$CO$_3$ CBL at different concentration of Cs$_2$CO$_3$, (c) Step by step illustration of deposition of SnO$_2$ and Cs$_2$CO$_3$ layers, (d) J-V characteristics of the current only device (inset device structure), (e) J−V characteristics, of the inverted P3HT: PC$_{60}$BM-based i-OSCs using different Cs$_2$CO$_3$ concentrations with SnO$_2$ as ETLs. Reproduced with permission from ref. [158]. Copyright © 2019, Elsevier B.V. All rights reserved.

3.2 Low work function metals as CBL

Jiang et al. [159] introduced the Ca as CBL in the device comprising of a P3HT: PCBM blend as the active layer. The conventional (ITO/MoO$_3$/P3HT: PCBM/Ca/Ag) and inverted (ITO/Ca/P3HT: PCBM/MoO$_3$/Au) device performance were compared. An enhancement of 29 % (Figure 12a) in the PCE and an increase of 750 % in the cell's shelf lifetime (Figure 12b) of the inverted device was reported than its conventional structure. An increased efficiency was achieved by reduced charge recombination at the active layer and electrode interface, and enhanced air-stability which was probably due to the better shielding of low work function metal anode in i-OSC architecture. The Ag, Al, and Mg metals also have been used to modify the ITO surface. These devices are categorized as A (without CBL), and B, C, D, and E, which are corresponding to modified ITO with Ag, Al, Mg, and Ca, respectively. Results depicted that Ca-based device has higher PCE as compared to Mg metal modified based devices, because Ca has lower work function than the rest of materials, and it helped in significantly improving the V$_{oc}$. Jouad et al. [160] reported the tris-(8-hydroxyquinoline)Aluminium (Alq$_3$) with Ca as CBL. They have shown the effect of layer by layer deposition of Ca/Alq$_3$, and the devices were fabricated by using the different thicknesses of Ca and Alq$_3$, whereCuPc/SubPc/C$_{60}$ was used as an active layer. In this case, ITO/Ca(x)/Alq$_3$(y)/active layer/ MoO$_3$/Al, was the device structure, and where x and y are the thickness in nm. The optimized PCE reported is 1.33 %, at 3 nm, and 6 nm thickness of Ca and Alq$_3$, respectively, as compared to PCE~1.02 % for Ca (3 nm)/Alq$_3$ (0 nm). It shows the coating of Alq$_3$ on top of Ca has improved the charge extraction, and resulted in an improvement of the device performance.
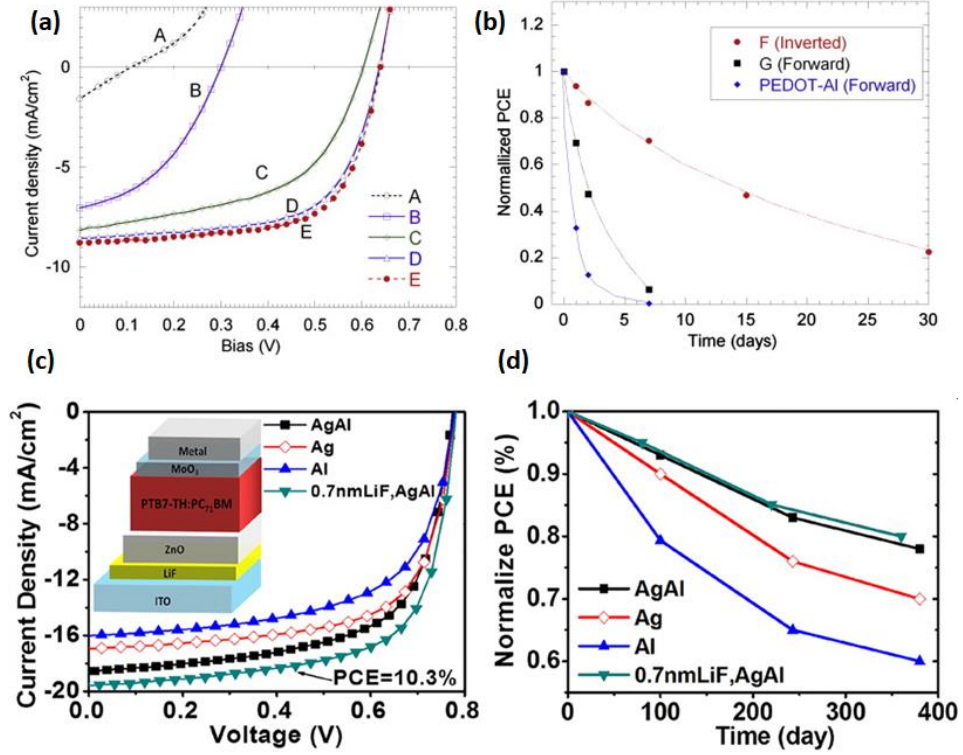
Figure (12): (a) J- V characteristics of the i-OSCs device; where, A is bare ITO substrate, and B, C, D, and E are modified ITO with Ag, Al, Mg, and Ca, respectively, and (b) stability measurement of conventional and inverted devices. Reproduced with permission from ref. [159] Copyright © 2010, Elsevier B.V. All rights reserved. (c) J-V characteristics of devices with different top electrodes under illumination (inset the device structure), (d) The device PCE versus time (days) plot of different electrode devices. Reproduced with permission from ref.[161] Copyright © 2016, American Chemical Society .

Table 5: Low work function metals, quantum dots, and metal oxides CBL based inverted devices performance parameters.

Device structure	Active layer	CBL	V_{oc} (V)	J_{sc} (mA/cm^2)	FF	PCE (%)	Ref.

ITO/CBL/Active layer/ MoO$_3$/Au	P3HT: PCBM	-	0.11	1.57	0.23	0.04	[159]
		Ca	0.64	8.78	0.65	3.67	
ITO/CBL/Active layer/ MoO$_3$/Ag	P3HT: PCBM	RGO/TiO$_x$ (0 mg/mL)	0.66	8.54	0.54	3.03	[124]
		RGO/TiO$_x$ (0.017 mg/mL)	0.66	8.80	0.56	3.25	
		RGO/TiO$_x$ (0.083 mg/mL)	0.64	9.85	0.61	3.82	
ITO/CBL/Active layer/ PEDOT: PSS/Au	MEH- PPV	PV	1.37	0.61	0.25	0.21	[129]
		In/PV	3.77	0.54	0.51	1.04	
		ZnO/PV	4.04	0.62	0.50	1.24	
FTO/CBL/Active layer/ MoO$_3$/Ag	P3HT: PCBM	ZnO (0.75 M)	0.60	5.98	0.47	1.71	[118]
		ZnO (0.5 M)	0.60	6.94	0.53	2.24	
		ZnO (0.3 M)	0.62	8.08	0.57	2.84	
		ZnO (0.1 M)	0.61	8.85	0.57	3.09	
FTO/CBL/Acive layer/ PEDOT: PSS/ Ag	P3HT: PCBM	TiO$_2$	0.57	8.95	0.53	2.80	[146]
		Nb$_2$O$_3$	0.60	7.94	0.55	2.70	
ITO/ CBL/	P3HT:	Al$_2$O$_3$	9.34	0.63	0.62	3.66	[64]

Active layer/ MoO$_3$/Al	PCBM	ZnO	8.03	0.62	0.61	3.05	
		e-Al$_2$O$_3$	8.90	0.63	0.63	3.60	

3.3 Alkali metal compounds as CBL

The LiF-modified ITO substrate have been reported for i-OSCs, owing to its formation of very thin layer and it shows good conductivity as well as transparency. [162] Jia et al.[161] have achieved PCE of 10 % by introducing an ultrathin LiF layer between ITO and ZnO as a CBL for PTB7-Th: PC$_{71}$BM blend system, in the ITO/LiF/ZnO/PTB7-Th: PC$_{71}$BM/MoO$_3$/ (Al/Ag/AgAl) device structure. They also investigated the influence of the top electrode materials on device performance and the stability. The J-V characteristics (Figure 12c) of the device revealed that LiF (0.7 nm)/ZnO coating CBL with AgAl top electrode devices have shown the better performance than rest of the devices. A LiF coated ITO electrode helps to reduce the WF of ITO and improves the contact quality at ZnO/ITO interface. The enhacement of J$_{sc}$ and FF of LiF-modified ITO electrode device can suggest the improvement of electron extraction in the OSCs. Table (6) has summarized the device performance parameters at different LiF thickness for AgAl top electrode OSCs. The device without LiF and AgAl top electrodes had V$_{oc}$ of 0.78 V, J$_{sc}$ of 18.2 mA/cm^2, FF of 0.66, and the PCE of 9.3 %, which is lowered than PCE (10.3 %) delivered by LiF based devices. The device stability (Figure 12d) with longer life was found for LiF based device and with AgAl top electrode. The average PCE of cells with a top electrode of Ag$_{92}$Al$_8$ (8wt % Al) was 9.1 %. As author suggested the AgAl top electrode attribute to higher reflectivity and as a result higher absorption in the active layer compared to Al and Ag top electrodes devices were observed. Balderrama et al. [163] also applied the ultrathin 0.5-0.8 nm film of thermally deposited LiF layer in PBDTTT-EFT: PC$_{70}$BM low bandgap donor blend system based

device. The optimized device (ITO/LiF/PFN/PBDTTT-EFT: $PC_{70}BM/V_2O_5/Ag$) yielded a PCE of 11 % with the highest FF of 0.73.

Table 6: Alkali metal compounds and graphene quantum dots CBL based devices parameters summary.

Device structure	Active layer	CBL	V_{oc} (V)	J_{sc} (mA/cm^2)	FF	PCE (%)	Ref.
ITO/CBL/ Active layer /MoO$_3$/AgAl	PTB7-Th: PC$_{71}$BM	-	0.78	18.20	0.66	9.30	[161]
		LiF (0.7 nm)/ZnO	0.78	19.50	0.67	10.30	
		LiF (1.1 nm)/ZnO	0.78	18.80	0.66	9.70	
		LiF (1.5 nm)/ZnO	0.78	17.80	0.66	9.20	
ITO/CBL/ Active layer/ MoO$_3$/ Au	P3HT: PCBM	GQDs	0.50	4.70	0.33	0.79	[164]
		Cs$_2$CO$_3$	0.57	8.37	0.54	2.59	
		GQDs-Cs$_2$CO$_3$	0.58	9.04	0.60	3.17	

3.4 Organic materials as CBL

Small- molecules

In 2004, Sahin et al. [165] used perylene diimide (or bathocuproine (BCP) as CBL which was deposited via thermally evaporation method on top of the ITO substrate. The fabricated devices (Figure 13a) comprised of MEH-PPV: PCBM active layer and CuPc as a HTL layer. BCP based OSCs (Figure 13c) have shown the improvement in the J_{sc} than control device (Figure 13b). The BCP was also explored by many researchers with different blend based devices. [103,166] In 2018, Zheng et al. [167], introduced a *n*-type small molecule POF-N as CBL which comprises of multi-amino groups and acted as an electron-deficient conjugated backbone with relatively good electron transport properties than the other cathode interlayer materials with *p*-type backbone. The POF-N was doped into active layer, and coated as single layer via single step coating. Interestingly, the POF-N coating based inverted device yielded comparable PCE to ZnO CBL based device, both had PTB7-Th: $PC_{71}BM$ as an active layer. The enhanced PCE can be attributed to the fact that POF-N preferably aggregates closely on the ITO surface during its coating process and serves as the CBL. The optimized device obtained at 1 % weight ratio of POF-N in PTB7-Th (1 % POF-N: PTB7-Th: $PC_{71}BM$), and single step coated device exhibited best PCE up to 10.0 %. The two-step method which includes the separate coating of POF-N interlayer and PTB7-Th: $PC_{71}BM$ blend system device (POF-N/PTB7-Th: $PC_{71}BM$), delivered the PCE up to 9.5 %, and which was lower than one-step coating method. They also reported the device with non-fullerene (PBDB-T: ITIC) and all polymer (PTzBI: N2200) blend system with the same configuration. For PTB7-Th: $PC_{71}BM$, PBDBT: ITIC, and PTzBi: N2200 blend system, the optimized results (PCE) were reported at optimum weight ratio of 1 wt% POF-N in active layer, which were 10 %, 10 %, and 6.5 %, respectively. This was an enormous improvement in comparsion to control devices. However, for PBDBT-T: ITIC blend system, performance was comparable for both single step and double step processing device. Whereas, for PTzBI: N2200

blend systems the device performance was reduced in case of one step coating process of 1 wt % POF-N in active layer and the highest PCE 6.5 % reported and it was lower as compared to two step processing (PCE~ 7 %). The cause of reduction of performance of PTzBI: N2200 blend based on one step processing devices can be explained due to the increase in the surface roughness of active layer after introducing the 1 wt % POF-N in the blend. Author mentioned the increased RMS value from 0.75 (ITO/POF-N/PTzBI: N2200) to 1.64 nm (ITO/ POF-N (1 %)/ PTzBI: N2200). Li et al. [166] synthesized a CBL, called 4,7-diphenyl-1,10-phenanthroline-2,9-dicarboxylic acid (DPPA), and applied it as sole CBL and also used to modify the ZnO film. The DPPA was used in the P3HT: $PC_{61}BM$ based OSCs, an enhancement of 10 % in PCE (~3.55 %) of its initially value was observed in comparison to the control device (PCE~ 3.25 %). Moreover, DPPA was also used as the sole CBL, affording PCE enhancement due to the improved interfacial contact between the substrate and active layer.
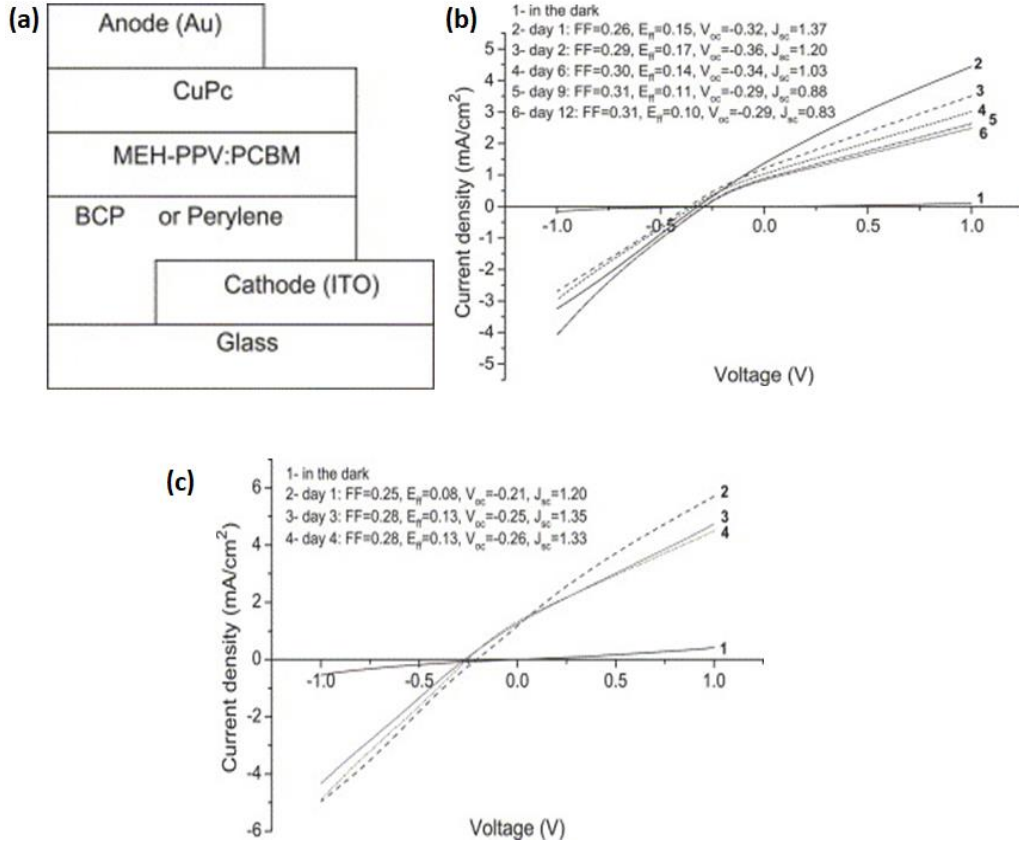
Figure (13): (a) The BCP CBL based inverted device structure, (b) J-V characteristic of device ITO/perylene diimide/MEH-PPV:PCBM/CuPC/Au OSCs under illumination, (c) J-V plot of device ITO/BCP/MEH-PPV: PCBM/CuPc/Au OSCs under illumination. Reproduced with permission from ref. [165]. Copyright © 2004 Elsevier B.V. All rights reserved

Polymers

The polyoxyethylene tridecyl ether (PTE) was introduced by Steim et al. [168] as an organic interface layer to improve the quality of the TiO_x layer. The P3HT: PCBM blend system was used in this study with PEDOT: PSS as the hole transport layer. A PCE of 3.6 % was achieved with ITO/PTE/TiO_x/blend device/PEDOT: PSS/Ag, which was higher than the control devices of ITO/TiOx/blend (PCE~ 3.1 %) and ITO/blend (PCE~ 1.6 %). The ultrathin PTE layer behaves as

an insulating layer, thereby enhances the shunt and reduces the series resistance, which increases the FF of the resultant device. Zhou et al. [169] introduced the polyethylene oxide (PEO) as a CBL to modify the ITO work function. The fabricated i-OSCs structure ITO/PEO/APFO-3: PCBM/PEDOT: PSS/PH500 have shown the high current and V_{oc} values as compared to a device without the PEO layer (PCE~ 0.37 %), and contributed higher PCE (~0.70 %) in PEO presence. The WF of ITO dropped from 4.4 to 3.9 eV after coating with PEO. The reduction of ITO work function contributed in the enhancement of V_{oc} for the PEO device. Another study on ITO work-function tuning was done by Na et al. [170] in 2010, in which they reported water-soluble polyfluorene (WPF-6-oxy-F) polymer CBL, and enhanced the performance of i-OSCs. The WPF-6-oxy-F dramatically raised the V_{oc} from 0.35 to 0.65 V, FF from 0.37 to 0.59, and J_{sc} from 8.05 to 8.83 mA/cm^2, and these contributed in the enhancement of PCE from 1.04 to 3.38 %. The device results show variation due to change in the thickness of WPF-6-oxy-F buffer layer, coated at the spin speed of 1000, 3000, 7000 rpm, and these correspond to 8.6, 3.4, and 2.1 nm thickness, respectively. The device parameters showed a reduction in values with increasing the buffer layer thickness. With increase in the MPE-6-oxy-F film thickness, reduction in the J_{sc} was seen due to increase in series resistance.. The alcohol-soluble 2,7-carbazole-1,4-phenylene copolymers, PCP-NOH and PCP-EP, comprising surfactant-like diethanolamino and phosphonate end groups on the side chains, respectively, were utilized as CBL on top of ITO to construct i-OSCs (Figure 14b) introduced by Zhu et al. [171]. The PCDTBT and PC$_{71}$BM were used as an donor, and acceptor, respectively in the device. PCP-NOH and PCP-EP shifted the ITO work function from 4.7 to 4.2 and 4.3 eV (Figure 14a), respectively, and thus improved in the electron extraction. The PCE of the i-OSCs without the CBL was 1.63 %, because of low V_{oc} of 0.48 V and FF of 0.36. The PCP-NOH and PCP-EP usage as CBL significantly enhanced V_{oc}

to 0.88 V and FF to 0.58, and delivered PCEs of 5.39 % and 5.48 %, respectively. The corresponding J-V plot of the device is shown in Figure 14(c). In another report, a solution-processable CBL of cationic biopolymer poly(2-(dimethylamino) ethyl methacrylate) (PDMAEMA) was used to modify the work function of ITO, and it was applied in P3HT: PCBM active layer based inverted device. It delivered the PCE of 3.3 % under AM1.5G illumination. The stability of PDMAEMA based devices in an ambient environment was better than ZnO CBL devices, as retention of 90 % of its PCE after 8 weeks was observed, and for this study initially the devices were illuminated in ambient condition under AM1.5G solar irradiation for 8 hrs and then kept in dark for rest of time. [172] It has been reported that photo-induced degradation occurs in ZnO layer and poor shunt resistance was recognized as the cause of degradation. [173] Whereas, the PDMAEMA does not suffer from photo-induced degradation phenomenon. [174] Another research group introduced a biopolymer poly (2-N,N-dimethylaminoethyl methacrylate) (PDMAEMA) as a solution-processable CBL in an i-OSCs. It contains tertiary amines, PDMAEMA can be easily protonated to form highly cationic polymers, and it reduces the WF of ITO (4.38 to 3.94 eV), thereby showing the ability of PDMAEMA to form strong interfacial dipoles due to its high cationic charges. Thus, it can overcome the issue of trap states, which are commonly found in metal oxides. The device comprised of P3HT:PCBM as active layer, MoO_3 as the top-hole selective layer, PDMAEMA as CBL, and silver as a top electrode. The PCE of 3.3 % was obtained, which is comparable with i-OSCs fabricated with ZnO as the CBL layer. The environmental stability improvement and enhanced lifetime of the device marks the importance of PDMAEMA as an alternative of ZnO in an i-OSCs. Recently Fu et al. [175] have modified the PDMAEMA and introduced a block copolymer into it and denoted by PF_{15}-b-$PDMAEMA_{75.}$ The device was fabricated with PTB7-Th: $PC_{71}BM$ blend system. Zhou

et al. [176] reported the universal method to reduce the WF of ITO by applying an ultrathin layer (1 to 10 nm) of polymers. The large bandgap, commercially available, air processable polymers were studied and applied in i-OSCs. The polymers used for the study were polyethylenimine ethoxylated (PEIE) and branched polyethylenimine (PEI). The value of the WF after depositing PEIE/PEI (10 nm) on substrates, buffer layer, and metal was measured by the UPS and Kelvin probe method. The WF values were reduced as compared to pristine substrate. Moreover, PEIE and PEI coated substrates were stable up to 190 ^{0}C, and 150 ^{0}C temperatures, respectively. Kyaw et al. [177] also reported the PEIE buffer layer, and it was sandwiched between ZnO and the active layer to form the ITO/ZnO/PEIE/p-DTS(FBTTh$_2$)$_2$: PC$_{71}$BM/MoO$_3$/Ag device structure. The ZnO interlayer work function was approximately 4.5 eV as measured from the Kelvin probe method, and after coating the PEIE on top of ITO/ZnO the resultant work function was reduced to 3.8 eV. The PEIE film created a dipole moment due to the presence of neutral amine groups at the interface and that helped to shift energy level by 0.7 eV. [176] Similarly, the coated film of PEIE above ITO also effectively changed the work function from 5.1 to 4.1 eV of the ITO substrate. The PEIE coating has also helped to reduce the ZnO film surface roughness. As a result, the PEIE improved the device's J$_{sc}$ as well as FF, as shown in the J-V characteristics (Figure 14(d)). The ITO/ZnO, ITO/PEIE, and ITO/ZnO/PEIE coated devices delivered PCE up to 6.29, 5.18, and 7.88 %, respectively. Thus, after both buffer layer coating (layer by layer), the film surface and work function were influenced and hence directly affected the J$_{sc}$ and FF.
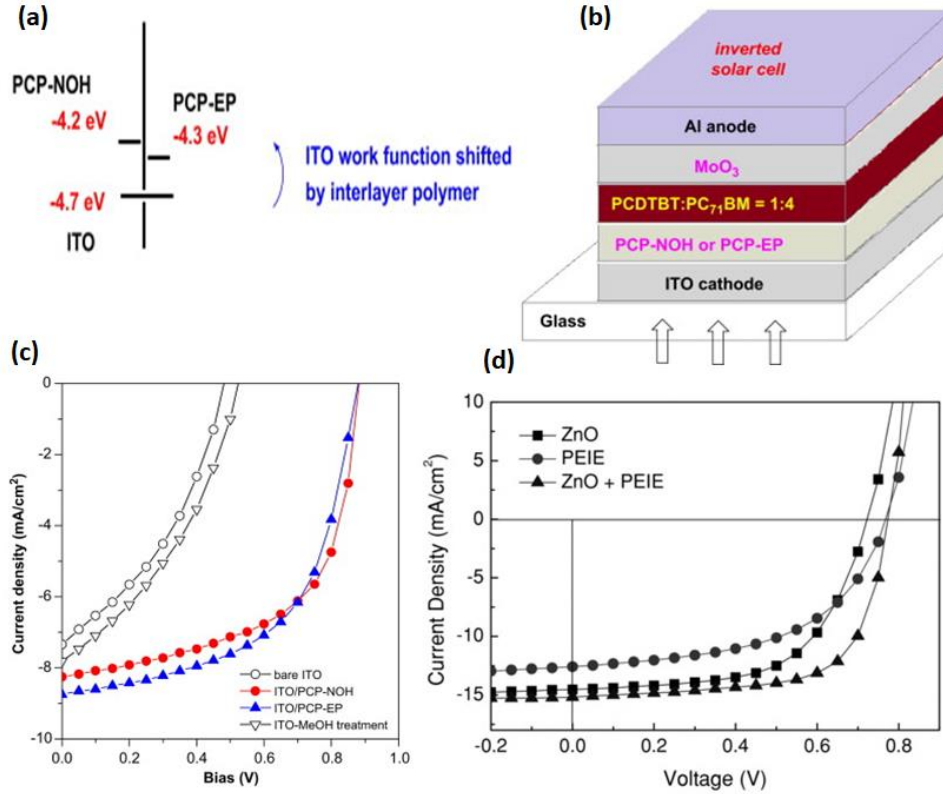
Figure (14): (a) ITO work function modified diagram, after coating the polymer CBL on top of ITO substrates, (b) PCP-NOH/PCP-EP coated CBL based inverted device structure configuration, and (c) J-V plot of the resultant device under AM1.5 illumination. Reproduced with permission from ref. [171]. Copyright © 2011, Elsevier B.V. All rights <mark>reserved.</mark> (d) J-V curve of OSCs (ITO/CBL/p-DTS(FBTTh$_2$)$_2$: PC$_{70}$BM/MoO$_3$/Ag), with an interlayer of PEIE, ZnO, and ZnO/PEIE, measured under AM1.5 G illumination. Reproduced with permission from ref. [177]. Copyright @ WILEY-VCH Verlag GmbH & Co. KGaA, Weinheim, 2013.

Liu et al. [178] introduced the amino-functionalized conjugated metallopolymers named PFEO-Hg, PFEN, PFN-OX, and PFEN-Hg, as CBL in i-OSCs with PTB7: PC$_{71}$BM blend system. The PFEO-Hg, PFEN, PFN-OX, and PFEN-Hg have improved the device PCE of 5.98, 8.80, 9.03, and 9.11 %, respectively. It was a huge enhancement than control device (3.18 %). The alcohol

or water-soluble interlayer polymer poly[(9,9-bis(3′-(N,N-dimethylamino)propyl)-2,7-fluorene)-alt-2,7-(9,9–dioctylfluorene)] (PFN) was also widely used as CBL, and it is either coated as single or incorporated with metal and polymer buffer layers. Zhang et al. [179] also reported the water and alcohol soluble buffer layer for i-OSCs, and these CBLs are abbreviated as FBF-N and FTBTF-N. The CBLs were coated as per ITO/CBL/PTB7: $PC_{71}BM/MoO_3/Al$ device structure. The FBF-N and FTBTF-N CBLs helped to achieve the PCE up to 7.97 and 9.22 %, respectively, as compared to bare ITO based device (PCE~ 1.18 %).

Fullerene derivatives

Fullerene derivatives are well studied as acceptor molecules in the development of OSCs, and recently it is also studied as inter layers for highly efficient i-OSCs. Gong et al. [180] introduced the two novel fullerene derivative molecules named as FBPNOH, and FPNOH as CBL. Both have shown the favorable WF of 3.80 and 3.59 eV, for ITO/EPNOH and ITO/FBPNOH films, respectively. The thermal annealing (TA) as well as solvent annealing (SA) techniques have been applied to modify the property of the CBL layer. For SA, the film was first processed through TA (100 ^{o}C) and then treated by SA process. The ITO/FPNOH showed the film roughness (RMS) of 1.42 and 1.39 nm for TA and SA, respectively. ITO/FBPNOH film showed the RMS values of 1.26 and 1.20 for the TA and SA, respectively. In both the cases, SA improved the film roughness thereby improving the device performance. The device (ITO/CBL/PTB7-Th: $PC_{71}BM/MoO_3/Ag$) with EPNOH (TA) and FBPNOH (TA) has delivered the PCE of 9.66 % and 8.85 % respectively, which was higher than control device (with ZnO as CBL) performance (PCE~ 8.30 %). For SA, EPNOH and FBPNOH CBL based devices, the respective PCE up to 10.05 % and 9.49 % were found. The post-SA processing of these CBL have an impact on the

interfacial properties and charge transport ability. Thus, the corresponding device performance has been systematically improved.

3.5 Quantum dots (QDs) as CBL

The QDs with unique structural, morphological, optical, and electronic properties were also applied as CBL in i-OSCs. Lee et al. [181] introduced the solution-processable CdSe QDs as a CBL. It was coated on top of the ITO/Cs_2CO_3 layer as per $ITO/Cs_2CO_3/CdSe/P3HT:ICBA/MoO_3/Al$ device structure. The coating of CdSe QDs has decreased the WF of the cathode and reduced the series resistance. Resultant V_{oc} increased from 0.840 to 0.882 V, and FF improved from 0.635 to 0.687, which contributed to enhance the overall PCE from 4.61 to 5.20 %. The insertion of QDs also prevent the diffusion of Cs into the active layer, which improves the lifetime of the device. In 2013, Ho et al. [182] introduced the $CuGaSe_2$ (CGS) QDs on top of the ZnO buffer layer. The QDs formed the favourable energy level alignment between active layer and the ITO electrode. QDs also enhance the crystal quality of ZnO, thereby increasing photon absorption at shorter wavelength and leading to better carrier transport/collection. By employing these QDs as CBL, the PCE of the resultant device enhanced up to 4.11 % in comparison to the control device (PCE~ 3.32 %). Graphene quantum dots (GQDs), another emerging class of nanomaterials were used as CBL in i-OSCs. Yang et al. [183], introduced the Cs_2CO_3 functionalized GQDs (GQDs-Cs_2CO_3) as a CBL and due to the well matched energy levels between GQDs–cesium carbonate (GQDs–Cs_2CO_3) and it also modified the ITO work function. The PCE of GQDs–Cs_2CO_3 based device was approximately 22 % higher than Cs_2CO_3 CBL device. The device with GQDs–Cs_2CO_3 delivered PCE of 3.21 % than control device (PCE~ 2.39 %). All the three parameters J_{sc}, FF, as well as V_{oc} have improved from 7.44 to 9.18 mA/cm^2, 0.56 to 0.60, and 0.57 to 0.58 V, respectively. This can be attributed to the enhanced

exciton dissociation and suppressed free charge recombination at the cathode/polymer active layer interface by GQDs. [164] The J-V characteristics of the GQDs-CS$_2$CO$_3$ CBL device (Figure 15a), under illumination are shown in Figure 15(b), and also, the device performance parameters are summarized in Table 6. The results clearly show the enhancement of FF, and J$_{sc}$ after inserting the GQDs. Recently, Peng et al. [184] reported the potential of n-type tin oxide (n-SnO$_2$) as a CBL in fabricating high performance i-OSCs owing to its high electrical conductivity and low-temperature synthesis. Nonetheless, the surface defects on the solution-processed n-SnO$_2$ CBL were a serious factor in restricting the OSCs device performance. To overcome this defect related issue, InP/ZnS QDs were used for surface passivation of the n-SnO$_2$ layer. The solution-processed n-SnO$_2$/InP/ZnS QDs composite CBL exhibited better transmittance over the active layer absorption range, and showed good electrical conductivity. For comparison, n-SnO$_2$ and n-SnO$_2$/InP/ZnS QDs films were employed as CBL in the device architecture of ITO/CBL/PM6: Y6/MoO$_3$/Ag. The solar cell with n-SnO$_2$ layer exhibited a PCE of 13.86 %, with a V$_{oc}$, J$_{sc}$, and a FF of 0.814 V, 25.65 mA/cm^2, and 0.663, respectively. The RMS value of active layer reduced from 4.55 nm (ITO/n-SnO$_2$/PM6: Y6) to 2.72 nm (ITO/n-SnO$_2$/InP/ZnS/PM6:Y6). However, on using n-SnO$_2$/InP/ZnS QDs composite film as ETL, the device efficiency was improved from 13.86 % to 15. 22 % due to the improved morphology of PM6: Y6 layer. It enhanced the charge extraction and collection, and reduced the monomolecular recombination in the solar cell. As a result, n-SnO$_2$/InP/ZnS QDs CBL based device displays improved stability in comparison to the conventional device based on PEDOT: PSS. For stability test, the devices were kept for 500 hrs to complete the aging test. The PEDOT: PSS based device retains only 20 % PCE of its intial value, whereas, the n-SnO$_2$/InP/ZnS QDs CBL based inverted devices holds the 80 % of its intial value for the same period. Wang et al. [185] introduced the N, S-doped carbon quantum dots (N-

CQDs and N, S-CQDs), and doped it into ZnO. It formed the ZnO: N, S-CQDs composite ink, and it was applied as CBL in the ITO/CBL/PTB7-Th: PC$_{71}$BM/MoO$_3$/Al device structure. The N-CQDs worked as a surface modifier for ZnO film as well as a down-conversion layer, and it facilitated to convert incident UV light into visible and as a result, it also contributed towards more charge carriers generation in the active layer. Moreover, it did not show the light-soaking effect, and it passivated the O$_2$ vacancy defects of the ZnO surface as N-CQDs have an abundance of polar groups. The effect of UV-exposure on ZnO/ZnO: N-CQDs has also been investigated, and it showed a remarkable reduction in the work function of buffer layer. It was observed that the estimated work function of ZnO was 4.12 eV, and after UV-exposure, it was reduced to 3.94 eV, and the same trend was also reported for ZnO: N-CQDs film work function. The effect of UV-exposure on interlayers could be clearly seen from the measured J-V characteristics (Figure 15c). The device performance of ZnO without UV-exposure was lower than UV-exposed devices. Similarly, in the case of ZnO: N-CQDs, the device has shown PCE of 5.21 %, and after UV-exposure, PCE gets improved up to 9.06 %. However, in the case of ZnO: N, S-CQDs, the PCE was enhanced up to 9.36 % after UV-exposure than 9.31 % without UV. The pristine ZnO devices show the S-shaped kink in the J-V curve. In this report, the 365 nm UV light illumination was used which eliminated the S-shaped kink, and improved the device PCE from 4.67 to 9.18 % of ZnO device, owing to mainly improvement in FF from 0.36 to 0.68. Here, ZnO: N, S-CQDs based device has shown the soaking free J-V curve with high performance. In contrast to the undoped ZnO, the ZnO: N, S-CQDs suppressed the Shockley-Read-Hall or trap-assited recombination (Figure 15d). It implies the application of N,S-CQDs reduces the interfacial traps between ETL and active layer interface. The roughness (RMS) of ZnO film was reduced from 2.57 nm to 2.16 nm after modifying it with N, S-CQDs quantum

dots. It implies that N-CQDs/N, S-CQDs quantam dots are capable of passivating the defects on the surface of ZnO film. It also improved the contact behaviour between CBL and an active layer, thus resulting in suppression of the charge carrier recombination and helped in improving the over all device perrformance.
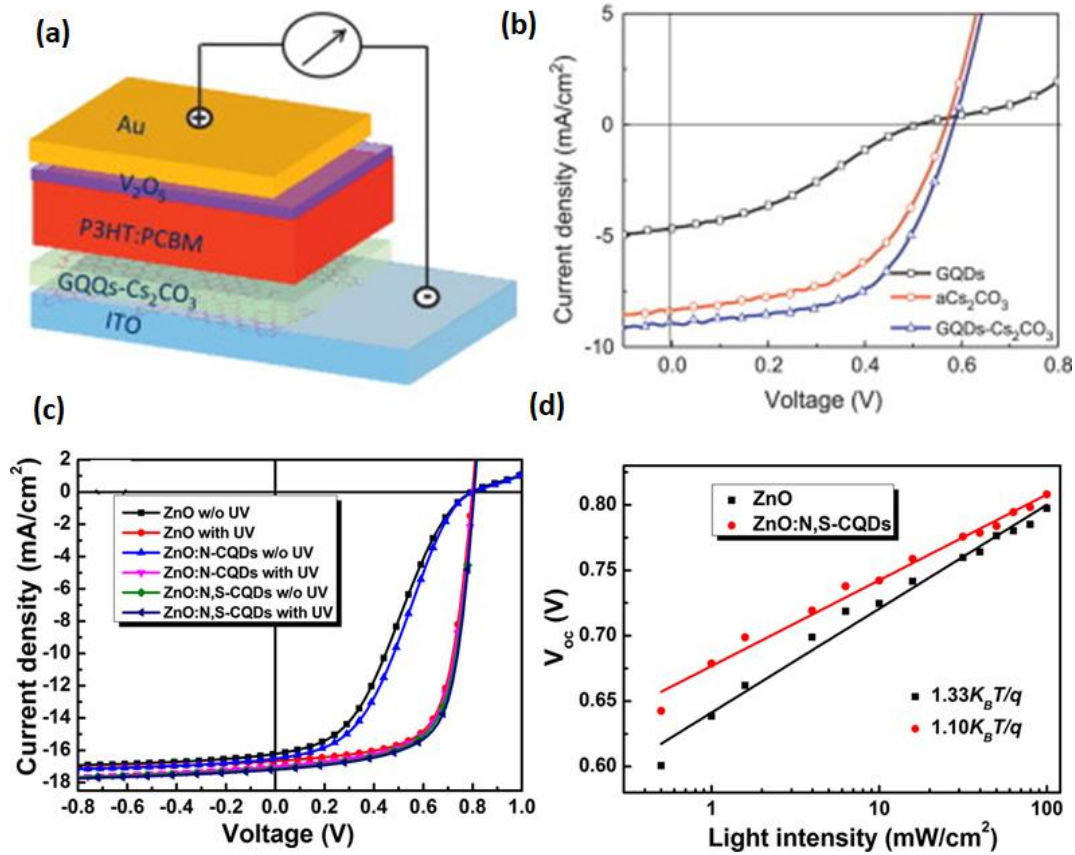

Figure 15: (a) Inverted OSC device structure with GQDs-Cs_2CO_3 as CBL, (b) J-V plot of the fabricated device with different QDs buffer layer under illumination. Reproduced with permission from ref. [164]. Copyright © 2013, Elsevier B.V. All rights reserved. (c) J-V characteristics of ZnO, and ZnO: N, S-CQDs buffer layer devices, (d) Semilogarithmic V_{oc}-

light intensity characteristics of the ZnO, and N,S-CQDs doped ZnO, based OSCs. Reproduced with permission from ref. [185]. Copyright © 2019, American Chemical Society.

4. Highly-efficient devices: Recently reported CBL

A variety of above mentioned CBL have resulted in extremely high-efficiency devices (>16%) along with improved stability. The OSC efficiency has touched a high mark of 18 % in the tandem configuration, with active layer materials PBDTS-TDZ:ITIC (80 nm) in the front cell and PTB7-Th:O6T4F:PC_{71}BM in the back cell with a thickness of 125 nm. The ZnO was the CBL material used in the device. Similarly, in other optimized two terminal tandem cells, an incredibly high PCE of 17.36 %, with a V_{oc} of 1.64 V, J_{sc} of 14.35 mA/cm^2 , and FF of 0.73, were attained. The CBL used in this case was ZnO/PFN-Br. Hence, in most of the recent highly efficient OSC devices, ZnO, ZnO:PFN-Br etc. were used as CBL. Besides this, other CBL materials explored recently in the high efficiency OSC devices are listed below in Table 7. The advantages of ZnO as CBL has been explained in detail in the above paragraph. A few organic molecules are also emerging as an advantageous CBL in OSCs as they does not require the thermal annealing step and are water/alcohol soluble, also compatible with polymer/small-molecule donors as well as with non-fullerene acceptor photoactive layers. [186,187] In organic molecules, the energy levels, electronic, and optical properties can be easily modified by making changes in the molecular structure. A self-assembled monolayer nature and intermolecular dipole movement make these an effective interlayer for device applications. These organic molecules based CBL can excellently reduce electrode work function, and lower the recombination, which thereby help in enhancing the charge collection and device voltage via forming dipole between the electrode and photoactive layer. [38] The PFN-Br is a well known conjugated polyelectrolytes (CPEs) molecule having two side chains of amino end groups and one main

chain backbone, with attached strong polar or ionic group to side chains which can produce a favorable interfacial dipole and helps in facilitating the electron injection and prevent recombination. [188] The PEI, and PEIE which comes under non-conjugted polyelectrolytes also have charged ionic groups. [189] The solution-processed PEI helped to reduce the electrode work function as well as form strong self-assembled dipoles at the cathode. A PDINO small molecule is a CBL material reported in high efficient conventional devices, and it contains perylene diimides as core and amino N-oxide as a terminal substituent. The Phen-NaDPO has also been reported and it has shown the excellent solubility in common solvents as well as has high electron mobility. [190] Molecule PNDIT-F3N and PNDIT-F3N-Br are also reported for high efficiency in tandem solar cells as CBL. These offer orthogonal solvent processability that is necessary for multilayer devices.

Table (7): Cathode buffer layers reported in highly efficient OSC with device structure.

S. No.	CBL	Device structure	Efficiency (%)	Ref.
1	ZnO	ITO/MoO$_3$/Tandem/ZnO/Electrode	18.6	[191]
2	PFN-Br	ITO/PEDOT: PSS/BHJ/PFN-Br/Al	17.3	[192]
3	ZnO	ITO/ZnO/BHJ/MoO$_3$/Ag	17.1	[193]
4	PFN-Br	ITO/PEDOT: PSS/BHJ/PFN-Br/Ag	17.0	[194]
5	ZnO:PFN-Br	ITO/ZnO/PFN-Br/Tandem/MoO$_x$/Ag	17.3	[195]
6	PNDIT-F3N	ITO/PEDOT: PSS/BHJ/PNDIT-F3N/Ag	16.8	[196]

7	Phen-NaDPO	ITO/PEDOT: PSS/BHJ/Phen-NaDPO/Ag	14.7	[197]
8	PDINO	PET/PEDOT: PSS/BHJ/PDINO/Al	14.1	[198]
9	ZnO:PEI	ITO/ZnO:PEI/BHJ/MoO$_3$/Ag	9.9	[199]

5. Conclusion and future perspective:

In this article, a detailed review of the OSCs devices with different CBL, and their performance has been summed up. In addition, this article also provides an overview of the OSCs basics, and their detailed functioning. In recent years a lot of research has been done on exploring the novel CBL materials with a detailed understanding of the interface processes in order to enhance PCE along with prolonged device stability at low-cost fabrication as well as suitable for scaling up mechanism. Hence, the CBL engineering is the need of time to improve the efficiency and compatibility with roll to roll processing of OSCs. The performances of different OSC devices have been compiled with different CBL materials. It was observed that the oxides and carbonates are popular as CBL in both conventional and inverted type OSCs. In metal oxides, ZnO is also one of the most widely used CBL in highly efficient i-OSCs as it has high reproducibility, chemical and thermal stabity, low temperature and solution processability, and have favorable electronic and optical properties, etc. Metals and alkali metal fluorides, including Ca, Ba, and LiF, are also popular as CBL especially Ca and Ba, which help in electron extraction and improve the PCE by reducing the interfacial recombination losses and modulating the electrode work-function. LiF is a well-known CBL material which results in dipole moment generation across the junction, possibly due to its orientation or due to the chemical reactions occurring at

interface, resulting in charge transfer and thus improves the efficiency. Similarly, NaF, CsF, and KF, etc., have also been explored as CBL materials, and considerable improvements have been achieved in device performance. Organic molecule-based CBL materials such as BCP, CuPc, TIPD, etc. are also popular choices that help in improving the device performance. Quantum dots of graphene, CdSe, ZnS, InP, Si, etc. have also been used recently as CBL for different OSCs and have contributed to PCE enhancement with their improved photonic and electric properties. The choice of CBL also depends on the properties of active layer material and device structures. Still, the low PCE and stability are the two big hurdles in OSCs commercialization. The efficiency of OSCs is also restricted due to their narrow absorption range and spectral mismatch issues. The UV and IR photons in the incident solar spectrum are still not useful for OSCs, and the UV photons of high energy lead to photo-induced degradation in the photoactive layer. It reduces the lifetime of devices. The luminescent spectral modifiers can be used to resolve this spectral mismatch related issue in the OSCs. The spectral converter material doped CBL layer not only contributes in charge carrier extraction and absorption broadening, but also protects the active layer from high energy incident photons. A variety of such lanthanides and non-lanthanide based spectral convertors have been used in various photovoltaic technology such as DSSC, OSCs, silicon, and perovskites. Hence, in the future, the dual function CBL could be useful. It could solve a spectral mismatch issue as well as protect the device from harmful UV. The composites of two or more above mentioned CBL materials can also be employed as CBL for further improving the performance and stability of the OSC devices. In summary the review suggested the importance of different CBL and their role in efficiency as well as stability.

Acknowledgment

References:

[1]   W. F. Lamb, T. Wiedmann, J. Pongratz, R. Andrew, M. Crippa, J. G. J. Olivier, D. Wiedenhofer, G. Mattioli, A. Al Khourdajie, J. House, S. Pachauri, M. Figueroa, Y. Saheb, R. Slade, K. Hubacek, L. Sun, S. K. Ribeiro, S. Khennas, S. de la Rue du Can, L. Chapungu, S. J. Davis, I. Bashmakov, H. Dai, S. Dhakal, X. Tan, Y. Geng, B. Gu, J. Minx, *Environ. Res. Lett.* **2021**, *16*, 073005.

[2]   I. Mpacts, A. Daptation, V. Ulnerability, *Choice Rev. Online* **2002**, *39*, 39.

[3]   T. S. Liang, M. Pravettoni, C. Deline, J. S. Stein, R. Kopecek, J. P. Singh, W. Luo, Y. Wang, A. G. Aberle, Y. S. Khoo, *Energy Environ. Sci.* **2019**, *12*, 116.

[4]   P. Chelvanathan, M. I. Hossain, N. Amin, *Curr. Appl. Phys.* **2010**, *10*, S387.

[5]   S. S. Chu, T. L. Chu, F. S. Zhang, L. Book, J. M. Yu, *Appl. Phys. Lett.* **1981**, *39*, 803.

[6]   G. Fulop, M. Doty, P. Meyers, J. Betz, C. H. Liu, *Appl. Phys. Lett.* **1982**, *40*, 327.

[7]   M. Nath, P. Chatterjee, J. Damon-Lacoste, P. Roca i Cabarrocas, *J. Appl. Phys.* **2008**, *103*, 034506.

[8]   R. W. Miles, G. Zoppi, I. Forbes, *Mater. Today* **2007**, *10*, 20.

[9]   A. Mohammad Bagher, *Int. J. Renew. Sustain. Energy* **2014**, *3*, 53.

[10]   M. A. Green, A. Ho-Baillie, H. J. Snaith, *Nat. Photonics* **2014**, *8*, 506.

[11]   P. P. Kumavat, P. Sonar, D. S. Dalal, *Renew. Sustain. Energy Rev.* **2017**, *78*, 1262.

[12]   J. Wu, Z. Lan, J. Lin, M. Huang, Y. Huang, L. Fan, G. Luo, *Chem. Rev.* **2015**, *115*, 2136.

[13]   N. R. Champness, *Dalt. Trans.* **2011**, *40*, 10311.

[14]   J. Jeong, M. Kim, J. Seo, H. Lu, P. Ahlawat, A. Mishra, Y. Yang, M. A. Hope, F. T. Eickemeyer, M. Kim, Y. J. Yoon, I. W. Choi, B. P. Darwich, S. J. Choi, Y. Jo, J. H. Lee, B. Walker, S. M. Zakeeruddin, L. Emsley, U. Rothlisberger, A. Hagfeldt, D. S. Kim, M. Grätzel, J. Y. Kim, *Nature* **2021**, *592*, 381.

[15] W. Ke, M. G. Kanatzidis, *Nat. Commun.* **2019**, *10*, 965.

[16] R. Kour, S. Arya, S. Verma, J. Gupta, P. Bandhoria, V. Bharti, R. Datt, V. Gupta, *Glob. Challenges* **2019**, 1900050.

[17] F. He, L. Yu, *J. Phys. Chem. Lett.* **2011**, *2*, 3102.

[18] Y.-J. Cheng, S.-H. Yang, C.-S. Hsu, *Chem. Rev.* **2009**, *109*, 5868.

[19] G. Li, V. Shrotriya, J. Huang, Y. Yao, T. Moriarty, K. Emery, Y. Yang, *Nat. Mater.* **2005**, *4*, 864.

[20] S. K. Hau, H.-L. Yip, A. K.-Y. Jen, *Polym. Rev.* **2010**, *50*, 474.

[21] R. Po, C. Carbonera, A. Bernardi, N. Camaioni, *Energy Environ. Sci.* **2011**, *4*, 285.

[22] G. Li, R. Zhu, Y. Yang, *Nat. Photonics* **2012**, *6*, 153.

[23] R. F. Service, *Science (80-.).* **2011**, *332*, 293.

[24] Y. Li, G. Xu, C. Cui, Y. Li, *Adv. Energy Mater.* **2018**, *8*, 1701791.

[25] S. E. Root, S. Savagatrup, A. D. Printz, D. Rodriquez, D. J. Lipomi, *Chem. Rev.* **2017**, *117*, 6467.

[26] V. Y. Merritt, H. J. Hovel, *Appl. Phys. Lett.* **1976**, *29*, 414.

[27] C. W. Tang, *Appl. Phys. Lett.* **1986**, *48*, 183.

[28] H. Spanggaard, F. C. Krebs, *Sol. Energy Mater. Sol. Cells* **2004**, *83*, 125.

[29] A. J. H. G. Yu,* J. Gao, J. C. Hummelen, F. Wudi, *Science (80-.).* **1995**, *270*, 1.

[30] Y. Cui, H. Yao, J. Zhang, K. Xian, T. Zhang, L. Hong, Y. Wang, Y. Xu, K. Ma, C. An, C. He, Z. Wei, F. Gao, J. Hou, *Adv. Mater.* **2020**, *32*, 1908205.

[31] J. Drechsel, B. Männig, D. Gebeyehu, M. Pfeiffer, K. Leo, H. Hoppe, *Org. Electron.* **2004**, *5*, 175.

[32] X. Crispin, *Sol. Energy Mater. Sol. Cells* **2004**, *83*, 147.

[33]   H. Frohne, S. E. Shaheen, C. J. Brabec, D. C. Müller, N. S. Sariciftci, K. Meerholz, *ChemPhysChem* **2002**, *3*, 795.

[34]   W. Li, Q. Song, X. Sun, M. Wang, H. Wu, X. Ding, X. Hou, *Sci. China Physics, Mech. Astron.* **2010**, *53*, 288.

[35]   X. Li, W. Zhang, K. Usman, J. Fang, *Adv. Energy Mater.* **2018**, *8*, 1702730.

[36]   H.-L. Yip, A. K. Y. Jen, *Energy Environ. Sci.* **2012**, *5*, 5994.

[37]   S. Ye, Z. Liu, Z. Bian, C. Huang, *Acta Chim. Sin.* **2015**, *73*, 193.

[38]   Z. Yin, J. Wei, Q. Zheng, *Adv. Sci.* **2016**, *3*, 1500362.

[39]   M.-H. Jao, H.-C. Liao, W.-F. Su, *J. Mater. Chem. A* **2016**, *4*, 5784.

[40]   C. Cui, Y. Li, Y. Li, *Adv. Energy Mater.* **2017**, *7*, 1601251.

[41]   J. Vinokur, B. Shamieh, I. Deckman, A. Singhal, G. L. Frey, *Chem. Mater.* **2016**, *28*, 8851.

[42]   B. Xu, J. Hou, *Adv. Energy Mater.* **2018**, *8*, 1800022.

[43]   G. Lastra, V. S. Balderrama, L. Resendiz, J. Pallares, S. I. Garduno, V. Cabrera, L. F. Marsal, M. Estrada, *IEEE J. Photovoltaics* **2018**, *8*, 505.

[44]   C.-C. Chueh, C.-Z. Li, A. K. Y. Jen, *Energy Environ. Sci.* **2015**, *8*, 1160.

[45]   P. Rappaport, *Sol. Energy* **1959**, *3*, 8.

[46]   J. Troughton, M. Neophytou, N. Gasparini, A. Seitkhan, F. H. Isikgor, X. Song, Y.-H. Lin, T. Liu, H. Faber, E. Yengel, J. Kosco, M. F. Oszajca, B. Hartmeier, M. Rossier, N. A. Lüchinger, L. Tsetseris, H. J. Snaith, S. De Wolf, T. D. Anthopoulos, I. McCulloch, D. Baran, *Energy Environ. Sci.* **2020**, *13*, 268.

[47]   C. Chen, S. Zhang, S. Wu, W. Zhang, H. Zhu, Z. Xiong, Y. Zhang, W. Chen, *RSC Adv.* **2017**, *7*, 35819.

[48]   S. Izawa, N. Shintaku, M. Kikuchi, M. Hiramoto, *Appl. Phys. Lett.* **2019**, *115*, 153301.

[49] S. M. Menke, N. A. Ran, G. C. Bazan, R. H. Friend, *Joule* **2018**, *2*, 25.

[50] E.-H. Kim, C.-W. Yang, J.-W. Park, *J. Appl. Phys.* **2011**, *109*, 043511.

[51] Y. Gu, Z. Zhu, J. Song, H. Zeng, *Nanoscale* **2017**, *9*, 19374.

[52] K.-B. Kim, Y.-H. Tak, Y.-S. Han, K.-H. Baik, M.-H. Yoon, M.-H. Lee, *Jpn. J. Appl. Phys.* **2003**, *42*, L438.

[53] S. Schäfer, A. Petersen, T. A. Wagner, R. Kniprath, D. Lingenfelser, A. Zen, T. Kirchartz, B. Zimmermann, U. Würfel, X. Feng, T. Mayer, *Phys. Rev. B* **2011**, *83*, 165311.

[54] M. P. de Jong, L. J. van IJzendoorn, M. J. A. de Voigt, *Appl. Phys. Lett.* **2000**, *77*, 2255.

[55] G.-H. Kim, H.-K. Song, J. Y. Kim, *Sol. Energy Mater. Sol. Cells* **2011**, *95*, 1119.

[56] X. Crispin, S. Marciniak, W. Osikowicz, G. Zotti, A. W. D. van der Gon, F. Louwet, M. Fahlman, L. Groenendaal, F. De Schryver, W. R. Salaneck, *J. Polym. Sci. Part B Polym. Phys.* **2003**, *41*, 2561.

[57] J. van de Lagemaat, T. M. Barnes, G. Rumbles, S. E. Shaheen, T. J. Coutts, C. Weeks, I. Levitsky, J. Peltola, P. Glatkowski, *Appl. Phys. Lett.* **2006**, *88*, 233503.

[58] T. Yu, J. Xu, L. Liu, Z. Ren, W. Yang, S. Yan, Y. Ma, *J. Mater. Chem. C* **2016**, *4*, 9509.

[59] R. Steim, F. R. Kogler, C. J. Brabec, *J. Mater. Chem.* **2010**, *20*, 2499.

[60] H. Ma, H.-L. Yip, F. Huang, A. K. Y. Jen, *Adv. Funct. Mater.* **2010**, *20*, 1371.

[61] V. Gupta, A. K. K. Kyaw, D. H. Wang, S. Chand, G. C. Bazan, A. J. Heeger, *Sci. Rep.* **2013**, *3*, 1965.

[62] X. W. Sun, D. W. Zhao, L. Ke, A. K. K. Kyaw, G. Q. Lo, D. L. Kwong, *Appl. Phys. Lett.* **2010**, *97*, 1.

[63] F.-C. Chen, J.-L. Wu, S. S. Yang, K.-H. Hsieh, W.-C. Chen, *J. Appl. Phys.* **2008**, *103*, 103721.

[64] J. Peng, Q. Sun, Z. Zhai, J. Yuan, X. Huang, Z. Jin, K. Li, S. Wang, H. Wang, W. Ma,

Nanotechnology **2013**, *24*, 484010.

[65]   K. B. Sundaram, A. Khan, *J. Vac. Sci. Technol. A Vacuum, Surfaces, Film.* **1997**, *15*, 428.

[66]   F. J. Lim, Y. T. Set, A. Krishnamoorthy, J. Ouyang, J. Luther, G. W. Ho, *J. Mater. Chem. A* **2015**, *3*, 314.

[67]   M. O'Regan, Briab * and Gratzel, *Nature* **1991**, *253*, 737.

[68]   R. Peng, F. Yang, X. Ouyang, Y. Liu, Y.-S. Kim, Z. Ge, *Thin Solid Films* **2013**, *545*, 424.

[69]   T. Kuwabara, H. Sugiyama, T. Yamaguchi, K. Takahashi, *Thin Solid Films* **2009**, *517*, 3766.

[70]   K. Lee, J. Y. Kim, A. J. Heeger, In *Organic Photonic Materials and Devices VIII*; Grote, J. G.; Kajzar, F.; Kim, N., Eds.; 2006; Vol. 6117, p. 61170T.

[71]   J. Y. Kim, S. H. Kim, H.-H. Lee, K. Lee, W. Ma, X. Gong, A. J. Heeger, *Adv. Mater.* **2006**, *18*, 572.

[72]   J. K. Lee, N. E. Coates, S. Cho, N. S. Cho, D. Moses, G. C. Bazan, K. Lee, A. J. Heeger, *Appl. Phys. Lett.* **2008**, *92*, 243308.

[73]   M.-H. Park, J.-H. Li, A. Kumar, G. Li, Y. Yang, *Adv. Funct. Mater.* **2009**, *19*, 1241.

[74]   Y. Sun, C. J. Takacs, S. R. Cowan, J. H. Seo, X. Gong, A. Roy, A. J. Heeger, *Adv. Mater.* **2011**, *23*, 2226.

[75]   A. Hadipour, R. Müller, P. Heremans, *Org. Electron.* **2013**, *14*, 2379.

[76]   A. K. K. Kyaw, D. H. Wang, D. Wynands, J. Zhang, T. Q. Nguyen, G. C. Bazan, A. J. Heeger, *Nano Lett.* **2013**, *13*, 3796.

[77]   C.-Y. Chang, W.-K. Huang, J.-L. Wu, Y.-C. Chang, K.-T. Lee, C.-T. Chen, *Chem. Mater.* **2016**, *28*, 242.

[78]   Z. Tan, S. Li, F. Wang, D. Qian, J. Lin, J. Hou, Y. Li, *Sci. Rep.* **2015**, *4*, 4691.

[79]   F. J. Zhang, D. W. Zhao, Z. L. Zhuo, H. Wang, Z. Xu, Y. S. Wang, *Sol. Energy Mater.*

Sol. Cells **2010**, *94*, 2416.

[80] Y. Zhao, Z. Xie, Y. Qu, Y. Geng, L. Wang, *Synth. Met.* **2008**, *158*, 908.

[81] C. M. Proctor, T.-Q. Nguyen, *Appl. Phys. Lett.* **2015**, *106*, 083301.

[82] W. Ma, C. Yang, X. Gong, K. Lee, A. J. Heeger, *Adv. Funct. Mater.* **2005**, *15*, 1617.

[83] I. Hancox, E. New, T. S. Jones, *Org. Electron.* **2015**, *23*, 105.

[84] L. Yu, Q. Li, Z. Shi, H. Liu, Y. Wang, F. Wang, B. Zhang, S. Dai, J. Lin, Z. Tan, *ACS Appl. Mater. Interfaces* **2016**, *8*, 432.

[85] J. Huang, Z. Xu, Y. Yang, *Adv. Funct. Mater.* **2007**, *17*, 1966.

[86] J. Frisch, M. Schubert, E. Preis, J. P. Rabe, D. Neher, U. Scherf, N. Koch, *J. Mater. Chem.* **2012**, *22*, 4418.

[87] H. Ju, K. M. Knesting, W. Zhang, X. Pan, C.-H. Wang, Y.-W. Yang, D. S. Ginger, J. Zhu, *ACS Appl. Mater. Interfaces* **2016**, *8*, 2125.

[88] V. Gupta, L. F. Lai, R. Datt, S. Chand, A. J. Heeger, G. C. Bazan, S. P. Singh, *Chem. Commun.* **2016**, *52*, 8596.

[89] X. Peng, L. Hu, F. Qin, Y. Zhou, P. K. Chu, *Adv. Mater. Interfaces* **2018**, *5*, 1701404.

[90] F. Wang, Z. Tan, Y. Li, *Energy Environ. Sci.* **2015**, *8*, 1059.

[91] T. Aytun, A. Turak, I. Baikie, G. Halek, C. W. Ow-Yang, *Nano Lett.* **2012**, *12*, 39.

[92] C. J. Brabec, S. E. Shaheen, C. Winder, N. S. Sariciftci, P. Denk, *Appl. Phys. Lett.* **2002**, *80*, 1288.

[93] C. J. Brabec, S. E. Shaheen, C. Winder, N. S. Sariciftci, P. Denk, *Appl. Phys. Lett.* **2002**, *80*, 1288.

[94] E. Ahlswede, J. Hanisch, M. Powalla, *Appl. Phys. Lett.* **2007**, *90*, 163504.

[95] X. Jiang, H. Xu, L. Yang, M. Shi, M. Wang, H. Chen, *Sol. Energy Mater. Sol. Cells* **2009**,

93, 650.

[96] J. H. Park, T.-W. Lee, B.-D. Chin, D. H. Wang, O. O. Park, *Macromol. Rapid Commun.* **2010**, *31*, 2095.

[97] A. F. Mitul, J. Sarker, N. Adhikari, L. Mohammad, Q. Wang, D. Khatiwada, Q. Qiao, *AIP Adv.* **2018**, *8*, 025018.

[98] S. Chen, X. Du, G. Ye, J. Cao, H. Sun, Z. Xiao, L. Ding, *J. Mater. Chem. A* **2013**, *1*, 11170.

[99] P. Yang, S. Chen, Y. Liu, Z. Xiao, L. Ding, *Phys. Chem. Chem. Phys.* **2013**, *15*, 17076.

[100] M. Jeong, D. K. Moon, H. S. Kim, J. H. Kim, *J. Mater. Chem. C* **2020**, *8*, 15183.

[101] Y. Cai, L. Chang, L. You, B. Fan, H. Liu, Y. Sun, *ACS Appl. Mater. Interfaces* **2018**, *10*, 24082.

[102] C.-C. Chang, C.-F. Lin, J.-M. Chiou, T.-H. Ho, Y. Tai, J.-H. Lee, Y.-F. Chen, J.-K. Wang, L.-C. Chen, K.-H. Chen, *Appl. Phys. Lett.* **2010**, *96*, 263506.

[103] B. R. Patil, M. Ahmadpour, G. Sherafatipour, T. Qamar, A. F. Fernández, K. Zojer, H.-G. Rubahn, M. Madsen, *Sci. Rep.* **2018**, *8*, 12608.

[104] Z. Feng, Y. Hou, D. Lei, *Renew. Energy* **2010**, *35*, 1175.

[105] J.-H. Kim, S.-Y. Huh, T. Kim, H. H. Lee, *Appl. Phys. Lett.* **2008**, *93*, 143305.

[106] H. Du, Z. Deng, Z. Lü, Z. Chen, Y. Zou, Y. Yin, D. Xu, Y. Wang, *Thin Solid Films* **2011**, *519*, 4357.

[107] Z. Tan, C. Yang, E. Zhou, X. Wang, Y. Li, *Appl. Phys. Lett.* **2007**, *91*, 023509.

[108] J. Yu, N. Wang, Y. Zang, Y. Jiang, *Sol. Energy Mater. Sol. Cells* **2011**, *95*, 664.

[109] Y. Cai, L. Chang, L. You, B. Fan, H. Liu, Y. Sun, *ACS Appl. Mater. Interfaces* **2018**, *10*, 24082.

[110] D. Wang, W. Zeng, S. Chen, X. Su, J. Wang, H. Zhang, *Semicond. Sci. Technol.* **2015**, *30*,

085017.

[111] X. Zhao, C. Xu, H. Wang, F. Chen, W. Zhang, Z. Zhao, L. Chen, S. Yang, *ACS Appl. Mater. Interfaces* **2014**, *6*, 4329.

[112] W. Zhang, H. Wang, B. Chen, X. Bi, S. Venkatesan, Q. Qiao, S. Yang, *J. Mater. Chem.* **2012**, *22*, 24067.

[113] J. H. Jeon, D. H. Wang, H. Park, J. H. Park, O. O. Park, *Langmuir* **2012**, *28*, 9893.

[114] C.-Y. Kuo, M.-S. Su, Y.-C. Hsu, H.-N. Lin, K.-H. Wei, *Adv. Funct. Mater.* **2010**, *20*, 3555.

[115] M. Nam, S. Lee, J. Park, S.-W. Kim, K.-K. Lee, *Jpn. J. Appl. Phys.* **2011**, *50*, 06GF02.

[116] W.-H. Tseng, M.-H. Chen, J.-Y. Wang, C.-T. Tseng, H. Lo, P.-S. Wang, C.-I. Wu, *Sol. Energy Mater. Sol. Cells* **2011**, *95*, 3424.

[117] K.-S. Shin, H.-J. Park, B. Kumar, K.-K. Kim, S.-G. Ihn, S.-W. Kim, *J. Mater. Chem.* **2011**, *21*, 12274.

[118] A. K. K. Kyaw, X. W. Sun, C. Y. Jiang, G. Q. Lo, D. W. Zhao, D. L. Kwong, *Appl. Phys. Lett.* **2008**, *93*, 221107.

[119] D. Li, Y. Chen, P. Du, Z. Zhao, H. Zhao, Y. Ma, Z. Sun, *RSC Adv.* **2015**, *5*, 88973.

[120] Z. Lin, C. Jiang, C. Zhu, J. Zhang, *ACS Appl. Mater. Interfaces* **2013**, *5*, 713.

[121] H. Sun, J. Weickert, H. C. Hesse, L. Schmidt-Mende, *Sol. Energy Mater. Sol. Cells* **2011**, *95*, 3450.

[122] Y.-J. Kang, C. Su Kim, D. Sung You, S. Hoon Jung, K. Lim, D.-G. Kim, J.-K. Kim, S. Hyung Kim, Y.-R. Shin, S.-H. Kwon, J.-W. Kang, *Appl. Phys. Lett.* **2011**, *99*, 073308.

[123] A. Tayel, A. Ramadan, O. El Seoud, *Catalysts* **2018**, *8*, 491.

[124] Y. Zhang, S. Yuan, W. Liu, *Electrochim. Acta* **2014**, *143*, 18.

[125] D. Yang, P. Fu, F. Zhang, N. Wang, J. Zhang, C. Li, *J. Mater. Chem. A* **2014**, *2*, 17281.

[126] Y. Sun, J. H. Seo, C. J. Takacs, J. Seifter, A. J. Heeger, *Adv. Mater.* **2011**, *23*, 1679.

[127] C. S. Kim, S. S. Lee, E. D. Gomez, J. B. Kim, Y.-L. Loo, *Appl. Phys. Lett.* **2009**, *94*, 113302.

[128] S. Li, Z. Li, C. Liu, X. Zhang, Z. Zhang, W. Guo, L. Shen, S. Ruan, L. Zhang, *Phys. Chem. Chem. Phys.* **2017**, *19*, 15207.

[129] K. Takahashi, T. Nishi, S. Suzaka, Y. Sigeyama, T. Yamaguchi, J. Nakamura, K. Murata, *Chem. Lett.* **2005**, *34*, 768.

[130] Z. Liang, Q. Zhang, L. Jiang, G. Cao, *Energy Environ. Sci.* **2015**, *8*, 3442.

[131] T. Stubhan, H. Oh, L. Pinna, J. Krantz, I. Litzov, C. J. Brabec, *Org. Electron.* **2011**, *12*, 1539.

[132] H. Oh, J. Krantz, I. Litzov, T. Stubhan, L. Pinna, C. J. Brabec, *Sol. Energy Mater. Sol. Cells* **2011**, *95*, 2194.

[133] K.-S. Shin, K.-H. Lee, H. H. Lee, D. Choi, S.-W. Kim, *J. Phys. Chem. C* **2010**, *114*, 15782.

[134] A. K. K. Kyaw, X. Sun, D. W. Zhao, S. T. Tan, Y. Divayana, H. V. Demir, *IEEE J. Sel. Top. Quantum Electron.* **2010**, *16*, 1700.

[135] S. Bishnoi, V. Gupta, C. Sharma, D. Haranath, M. Kumar, S. Chand, *Org. Electron.* **2016**, *38*, 193.

[136] R. Datt, S. Bishnoi, R. Gupta, D. Haranath, S. N. Sharma, G. Gupta, S. Arya, S. Kumar, V. Gupta, *Synth. Met.* **2019**, *255*, 116112.

[137] Y. Wang, W. D. Xu, J. D. Zhang, L. Zhou, G. Lei, C. F. Liu, W. Y. Lai, W. Huang, *J. Mater. Chem. A* **2017**, *5*, 2460.

[138] Y. Wang, W. Xu, J. Yi, C. Zuo, Y. Gong, Y. Liu, W.-Y. Lai, W. Huang, *J. Mater. Chem. A* **2018**, *6*, 15977.

[139] Y. Gong, Z. Kan, W. Xu, Y. Wang, S. H. AlShammari, F. Laquai, W.-Y. Lai, W. Huang,

Sol. RRL **2018**, *2*, 1800120.

[140] Y. Chen, S. Chu, R. Li, Y. Qin, Y. Xu, X. Zhang, J. Wang, M. Liu, W.-Y. Lai, W. Huang, *Org. Electron.* **2019**, *66*, 1.

[141] X. Li, H. Wang, H. Nakayama, Z. Wei, J. A. Schneider, K. Clark, W.-Y. Lai, W. Huang, J. G. Labram, J. R. de Alaniz, M. L. Chabinyc, F. Wudl, Y. Zheng, *ACS Appl. Energy Mater.* **2019**, *2*, 3805.

[142] R. Datt, S. Arya, S. Bishnoi, R. Gupta, V. Gupta, A. Khosla, *Microsyst. Technol.* **2019**.

[143] K. Pandi, T. R. Naveen Kumar, S. K. Lakhera, B. Neppolian, *Energy Technol.* **2020**, *8*, 2000481.

[144] H. Jiang, T. Li, X. Han, X. Guo, B. Jia, K. Liu, H. Cao, Y. Lin, M. Zhang, Y. Li, X. Zhan, *ACS Appl. Energy Mater.* **2020**, *3*, 1111.

[145] C. Wang, D. Luo, Y. Gao, G. Wang, C. Wang, P. Ma, H. Li, S. Wen, W. Dong, S. Ruan, *J. Phys. Chem. C* **2019**, *123*, 16546.

[146] O. Wiranwetchayan, Z. Liang, Q. Zhang, G. Cao, P. Singjai, *Mater. Sci. Appl.* **2011**, *02*, 1697.

[147] Y. Zhou, H. Cheun, W. J. Potscavage, Jr, C. Fuentes-Hernandez, S.-J. Kim, B. Kippelen, *J. Mater. Chem.* **2010**, *20*, 6189.

[148] L. Qi, C. Zhang, Q. Chen, *Thin Solid Films* **2014**, *567*, 1.

[149] L. S. Pali, S. K. Gupta, A. Garg, *Sol. Energy* **2018**, *160*, 396.

[150] H. Fan, X. Zhu, *ACS Appl. Mater. Interfaces* **2016**, *8*, 33856.

[151] Y. Han, X. Chen, J. Wei, G. Ji, C. Wang, W. Zhao, J. Lai, W. Zha, Z. Li, L. Yan, H. Gu, Q. Luo, Q. Chen, L. Chen, J. Hou, W. Su, C. Q. Ma, *Adv. Sci.* **2019**, *6*, 1901490.

[152] J. T.-W. Wang, Z. Wang, S. Pathak, W. Zhang, D. W. DeQuilettes, F. Wisnivesky-Rocca-Rivarola, J. Huang, P. K. Nayak, J. B. Patel, H. A. Mohd Yusof, Y. Vaynzof, R. Zhu, I. Ramirez, J. Zhang, C. Ducati, C. Grovenor, M. B. Johnston, D. S. Ginger, R. J. Nicholas,

H. J. Snaith, *Energy Environ. Sci.* **2016**, *9*, 2892.

[153] Y. Bai, C. Zhao, R. Shi, J. Wang, F. Wang, T. Hayat, A. Alsaedi, Z. Tan, *Mater. Chem. Front.* **2020**, *4*, 2072.

[154] J. Huang, G. Li, E. Wu, Q. Xu, Y. Yang, *Adv. Mater.* **2006**, *18*, 114.

[155] G. Li, C.-W. Chu, V. Shrotriya, J. Huang, Y. Yang, *Appl. Phys. Lett.* **2006**, *88*, 253503.

[156] H.-H. Liao, L.-M. Chen, Z. Xu, G. Li, Y. Yang, *Appl. Phys. Lett.* **2008**, *92*, 173303.

[157] H. Kim, A. R. bin M. Yusoff, H. Lee, S. Lee, H. Kim, G. Seo, J. Youn, J. Jang, *Nanoscale Res. Lett.* **2014**, *9*, 323.

[158] V.-H. Tran, S. H. Eom, S. C. Yoon, S.-K. Kim, S.-H. Lee, *Org. Electron.* **2019**, *68*, 85.

[159] C. Y. Jiang, X. W. Sun, D. W. Zhao, A. K. K. Kyaw, Y. N. Li, *Sol. Energy Mater. Sol. Cells* **2010**, *94*, 1618.

[160] Z. El Jouad, L. Barkat, N. Stephant, L. Cattin, N. Hamzaoui, A. Khelil, M. Ghamnia, M. Addou, M. Morsli, S. Béchu, C. Cabanetos, M. Richard-Plouet, P. Blanchard, J. C. Bernède, *J. Phys. Chem. Solids* **2016**, *98*, 128.

[161] X. Jia, Z. Jiang, X. Chen, J. Zhou, L. Pan, F. Zhu, Z. Sun, S. Huang, *ACS Appl. Mater. Interfaces* **2016**, *8*, 3792.

[162] X. Liu, L. J. Guo, Y. Zheng, *Nanoscale Res. Lett.* **2017**, *12*, 543.

[163] V. S. Balderrama, J. G. Sánchez, G. Lastra, W. Cambarau, S. Arias, J. Pallarès, E. Palomares, M. Estrada, L. F. Marsal, *J. Mater. Chem. A* **2018**, *6*, 22534.

[164] H. Bin Yang, Y. Qian Dong, X. Wang, S. Yun Khoo, B. Liu, C. Ming Li, *Sol. Energy Mater. Sol. Cells* **2013**, *117*, 214.

[165] Y. Şahin, S. Alem, R. de Bettignies, J.-M. Nunzi, *Thin Solid Films* **2005**, *476*, 340.

[166] J. Li, X. Huang, J. Yuan, K. Lu, W. Yue, W. Ma, *Org. Electron.* **2013**, *14*, 2164.

[167] N. Zheng, Z. Wang, K. Zhang, Y. Li, F. Huang, Y. Cao, *J. Mater. Chem. A* **2019**, *7*, 1429.

[168]   R. Steim, S. A. Choulis, P. Schilinsky, C. J. Brabec, *Appl. Phys. Lett.* **2008**, *92*, 093303.

[169]   Y. Zhou, F. Li, S. Barrau, W. Tian, O. Inganäs, F. Zhang, *Sol. Energy Mater. Sol. Cells* **2009**, *93*, 497.

[170]   S.-I. Na, T.-S. Kim, S.-H. Oh, J. Kim, S.-S. Kim, D.-Y. Kim, *Appl. Phys. Lett.* **2010**, *97*, 223305.

[171]   Y. Zhu, X. Xu, L. Zhang, J. Chen, Y. Cao, *Sol. Energy Mater. Sol. Cells* **2012**, *97*, 83.

[172]   M. Jin Tan, S. Zhong, R. Wang, Z. Zhang, V. Chellappan, W. Chen, *Appl. Phys. Lett.* **2013**, *103*, 063303.

[173]   A. Manor, E. A. Katz, T. Tromholt, F. C. Krebs, *Adv. Energy Mater.* **2011**, *1*, 836.

[174]   P. Dubruel, E. Schacht, *Macromol. Biosci.* **2006**, *6*, 789.

[175]   J. Fu, L. Yuan, F. Ling, R. Duan, Q. Chen, H. Ma, M. Zhou, B. Song, Y. Zhou, Y. Li, *J. Power Sources* **2020**, *449*, 227474.

[176]   Y. Zhou, C. Fuentes-Hernandez, J. Shim, J. Meyer, A. J. Giordano, H. Li, P. Winget, T. Papadopoulos, H. Cheun, J. Kim, M. Fenoll, A. Dindar, W. Haske, E. Najafabadi, T. M. Khan, H. Sojoudi, S. Barlow, S. Graham, J.-L. Bredas, S. R. Marder, A. Kahn, B. Kippelen, *Science (80-.).* **2012**, *336*, 327.

[177]   A. K. K. Kyaw, D. H. Wang, V. Gupta, J. Zhang, S. Chand, G. C. Bazan, A. J. Heeger, *Adv. Mater.* **2013**, *25*, 2397.

[178]   S. Liu, K. Zhang, J. Lu, J. Zhang, H.-L. Yip, F. Huang, Y. Cao, *J. Am. Chem. Soc.* **2013**, *135*, 15326.

[179]   W. Zhang, Y. Wu, Q. Bao, F. Gao, J. Fang, *Adv. Energy Mater.* **2014**, *4*, 1400359.

[180]   Y. Gong, J. Zhang, B. Du, M. Wang, W.-Y. Lai, W. Huang, *ACS Appl. Electron. Mater.* **2019**, *1*, 854.

[181]   Y.-I. Lee, J.-H. Youn, M.-S. Ryu, J. Kim, J. Jang, *Org. Electron.* **2012**, *13*, 1302.

[182] C.-R. Ho, M.-L. Tsai, H.-J. Jhuo, D.-H. Lien, C.-A. Lin, S.-H. Tsai, T.-C. Wei, K.-P. Huang, S.-A. Chen, J.-H. He, *Nanoscale* **2013**, *5*, 6350.

[183] H. Bin Yang, Y. Q. Dong, X. Wang, S. Y. Khoo, B. Liu, *ACS Appl. Mater. Interfaces* **2014**, *6*, 1092.

[184] R. Peng, T. Yan, J. Chen, S. Yang, Z. Ge, M. Wang, *Adv. Electron. Mater.* **2020**, *6*, 1901245.

[185] Y. Wang, L. Yan, G. Ji, C. Wang, H. Gu, Q. Luo, Q. Chen, L. Chen, Y. Yang, C.-Q. Ma, X. Liu, *ACS Appl. Mater. Interfaces* **2019**, *11*, 2243.

[186] R. Wang, B. Wang, J. Wang, X. Zhang, D. Zhang, D. Wei, X. Sun, H. Zhou, Y. Zhang, *J. Mater. Chem. A* **2019**, *7*, 25808.

[187] L. Hu, Y. Liu, L. Mao, S. Xiong, L. Sun, N. Zhao, F. Qin, Y. Jiang, Y. Zhou, *J. Mater. Chem. A* **2018**, *6*, 2273.

[188] Y. Guo, H. Lei, C. Wang, J. Ma, C. Chen, X. Zheng, G. Yang, L. Xiong, Z. Tan, *Sol. RRL* **2020**, *4*, 1900482.

[189] H. Kang, S. Hong, J. Lee, K. Lee, *Adv. Mater.* **2012**, *24*, 3005.

[190] A. Seitkhan, M. Neophytou, M. Kirkus, E. Abou-Hamad, M. N. Hedhili, E. Yengel, Y. Firdaus, H. Faber, Y. Lin, L. Tsetseris, I. McCulloch, T. D. Anthopoulos, *Adv. Funct. Mater.* **2019**, *29*, 1905810.

[191] M. B. Salim, R. Nekovei, R. Jeyakumar, *Sol. Energy* **2020**, *198*, 160.

[192] L. Liu, Y. Kan, K. Gao, J. Wang, M. Zhao, H. Chen, C. Zhao, T. Jiu, A. -Y. Jen, Y. Li, *Adv. Mater.* **2020**, *32*, 1907604.

[193] Y. Lin, Y. Firdaus, M. I. Nugraha, F. Liu, S. Karuthedath, A. H. Emwas, W. Zhang, A. Seitkhan, M. Neophytou, H. Faber, E. Yengel, I. McCulloch, L. Tsetseris, F. Laquai, T. D. Anthopoulos, *Adv. Sci.* **2020**, *7*, 1.

[194] Y. Lin, B. Adilbekova, Y. Firdaus, E. Yengel, H. Faber, M. Sajjad, X. Zheng, E. Yarali,

A. Seitkhan, O. M. Bakr, A. El-Labban, U. Schwingenschlögl, V. Tung, I. McCulloch, F. Laquai, T. D. Anthopoulos, *Adv. Mater.* **2019**, *31*, 1902965.

[195] L. Meng, Y. Zhang, X. Wan, C. Li, X. Zhang, Y. Wang, X. Ke, Z. Xiao, L. Ding, R. Xia, H.-L. Yip, Y. Cao, Y. Chen, *Science (80-.).* **2018**, *361*, 1094.

[196] T. Liu, Y. Zhang, Y. Shao, R. Ma, Z. Luo, Y. Xiao, T. Yang, X. Lu, Z. Yuan, H. Yan, Y. Chen, Y. Li, *Adv. Funct. Mater.* **2020**, *30*, 2000456.

[197] H. Tang, H. Chen, C. Yan, J. Huang, P. W. K. Fong, J. Lv, D. Hu, R. Singh, M. Kumar, Z. Xiao, Z. Kan, S. Lu, G. Li, *Adv. Energy Mater.* **2020**, *2001076*, 2001076.

[198] W. Song, R. Peng, L. Huang, C. Liu, B. Fanady, T. Lei, L. Hong, J. Ge, A. Facchetti, Z. Ge, *iScience* **2020**, *23*, 100981.

[199] C. Liu, Z. Li, X. Zhang, W. Guo, L. Zhang, S. Ruan, *ACS Photonics* **2017**, *4*, 2952.